

The HERC2 ubiquitin ligase is essential for embryonic development and regulates motor coordination

Monica Cubillos-Rojas¹, Taiane Schneider¹, Ouadah Hadjebi¹, Leonardo Pedrazza^{1,2}, Jarbas Rodrigues de Oliveira², Francina Langa³, Jean-Louis Guénet³, Joan Duran⁴, Josep Maria de Anta⁴, Soledad Alcántara⁴, Rocio Ruiz^{5,6}, Eva María Pérez-Villegas⁶, Francisco J. Aguilar-Montilla⁶, Ángel M. Carrión⁶, Jose Angel Armengol⁶, Emma Baple⁷, Andrew H. Crosby⁷, Ramon Bartrons¹, Francesc Ventura¹ and Jose Luis Rosa¹

¹ Departament de Ciències Fisiològiques, IDIBELL, Campus de Bellvitge, Universitat de Barcelona, L'Hospitalet de Llobregat, Barcelona, Spain

² Laboratório de Pesquisa em Biofísica Celular e Inflamação, Pontifícia Universidade Católica do Rio Grande do Sul, Porto Alegre, Rio Grande do Sul, Brazil

³ Département de Biologie du Développement, Institut Pasteur, Paris, France

⁴ Departament de Patologia i Terapèutica Experimental, Campus de Bellvitge, Universitat de Barcelona, L'Hospitalet de Llobregat, Barcelona, Spain

⁵ Departamento de Bioquímica y Biología Molecular, Facultad de Farmacia, Universidad de Sevilla, Sevilla, Spain

⁶ Departamento de Fisiología, Anatomía y Biología Celular, Universidad Pablo de Olavide, Sevilla, Spain

⁷ Institute of Biomedical and Clinical Science, University of Exeter Medical School, RILD Wellcome Wolfson Centre, Exeter, UK

Correspondence to: Jose Luis Rosa, *email:* joseluisrosa@ub.edu

Keywords: ubiquitin, p53, Angelman syndrome, Purkinje cells, behavioural analysis, Pathology Section

Received: June 07, 2016

Accepted: August 01, 2016

Published: August 12, 2016

ABSTRACT

A mutation in the *HERC2* gene has been linked to a severe neurodevelopmental disorder with similarities to the Angelman syndrome. This gene codifies a protein with ubiquitin ligase activity that regulates the activity of tumor protein p53 and is involved in important cellular processes such as DNA repair, cell cycle, cancer, and iron metabolism. Despite the critical role of HERC2 in these physiological and pathological processes, little is known about its relevance *in vivo*. Here, we described a mouse with targeted inactivation of the *Herc2* gene. Homozygous mice were not viable. Distinct from other ubiquitin ligases that interact with p53, such as MDM2 or MDM4, p53 depletion did not rescue the lethality of homozygous mice. The HERC2 protein levels were reduced by approximately one-half in heterozygous mice. Consequently, HERC2 activities, including ubiquitin ligase and stimulation of p53 activity, were lower in heterozygous mice. A decrease in HERC2 activities was also observed in human skin fibroblasts from individuals with an Angelman-like syndrome that express an unstable mutant protein of HERC2. Behavioural analysis of heterozygous mice identified an impaired motor synchronization with normal neuromuscular function. This effect was not observed in p53 knockout mice, indicating that a mechanism independent of p53 activity is involved. Morphological analysis showed the presence of HERC2 in Purkinje cells and a specific loss of these neurons in the cerebella of heterozygous mice. In these animals, an increase of autophagosomes and lysosomes was observed. Our findings establish a crucial role of HERC2 in embryonic development and motor coordination.

INTRODUCTION

Angelman syndrome (AS) is a severe neurodevelopmental disorder that occurs in approximately one out of every 12,000 births. Patients with AS exhibit developmental delay, speech impairments, intellectual disability, epilepsy, abnormal electroencephalograms, puppet-like ataxic movements, prognathism, tongue protrusion, paroxysms of laughter, abnormal sleep patterns, hyperactivity, and a high prevalence of autism [1, 2]. Genetic studies revealed that AS is associated with maternal deletions of chromosome 15q11-q13, paternal chromosome 15 uniparental disomy, or rare imprinting defects that affect the transcription of genes within the 15q11-q13 region. Specific loss-of-function mutations in the maternally inherited *UBE3A* gene which resides within this chromosomal region have been identified in a subset of affected individuals [3]. The *UBE3A* gene encodes an E3 ubiquitin ligase called UBE3A or E6-associated protein (E6AP). More recently, a mutation in the *HERC2* gene has been linked to neurodevelopmental delay and dysfunction in both AS and autism-spectrum disorders among the Old Order Amish [4, 5]. Molecular analysis associated a missense mutation in the *HERC2* gene (c.1781C>T, p.Pro594Leu) with the disease phenotype. Although the *HERC2* gene also resides in the 15q11-q13 region, it seems that it is not imprinted [6]. *HERC2* encodes an ubiquitin ligase that binds to UBE3A and stimulates its ubiquitin ligase activity [7]. Deregulation of the activity of UBE3A is well recognized as contributing to the development of AS [2, 3]. Thus, disruption of *HERC2* function by this mutation is associated with a reduction in UBE3A activity resulting in neurodevelopmental delay with Angelman-like features [4, 5].

Genetic variations in the *HERC2* gene are associated with eye pigmentation. Although multiple genes contribute to eye colour in humans, most variation can be attributed to a strong interaction between *HERC2* and adjacent *OCA2* on chromosome 15 [8]. A distal regulatory element of the *OCA2* promoter is within intron 86 of the *HERC2* gene and three different sequence variants of *HERC2* have been identified, such as predictors of eye colour in humans [9, 10].

HERC2 belongs to the *HERC* gene family that encodes a group of proteins that contain multiple structural domains. All members have at least one copy of an N-terminal region showing homology to the cell cycle regulator RCC1 and a C-terminal HECT (homologous to the E6-AP carboxyl terminus) domain found in a number of E3 ubiquitin protein ligases. These two domains define the HERC family (HERC = HECT + RCC1) [11]. In humans, six members form the HERC family. They are classified into two groups: large (HERC1-2) and small (HERC3-6) proteins. Structurally, small HERC proteins contain the two characteristic domains HECT and RCC1, whereas large HERC proteins are giant proteins

(approximately 5,000 amino acid residues) containing additional domains, including several RCC1 domains. Functionally, the HERC protein family regulates ubiquitination and ISGylation processes associated with membrane trafficking, immune response, DNA repair, cell stress response and cancer biology [11-20]. Recently, several substrates of *HERC2* have been identified. *HERC2* targets ubiquitin-dependent proteasomal degradation to xeroderma pigmentosa A (XPA) during circadian control of nucleotide excision repair [21] and the breast cancer suppressor BRCA1 during the cell cycle [22]. These data, together with the interaction of *HERC2* with RNF8 [23], indicate a regulatory role for *HERC2* in DNA repair by nucleotide excision and by homologous recombination of DNA double-strand breakage. More recently, other substrates, such as NEURL4, USP33 or FBXL5, have been reported that also indicate the participation of *HERC2* in other important cellular processes such as centrosome architecture, β -adrenergic receptor recycling, RalB signaling, cancer cell migration, and iron metabolism [24-26].

HERC2 may also interact with proteins in a manner independent of proteasomal degradation. The tumor suppressor p53 is a transcription factor that coordinates the cellular response to several kinds of stress through the regulation of a wide range of genes [27, 28]. In response to stress, p53 transcriptional activation is dependent of its oligomerization state [29]. Thus, p53 mutations that impair its oligomerization have been associated with a rare hereditary cancer predisposition disorder called Li-Fraumeni syndrome [30, 31]. *HERC2* interacts with p53 and modulates its transcriptional activity by regulating its oligomerization [32]. RNA interference experiments showed that *HERC2* knock-down inhibited p53 oligomerization affecting its transcriptional activity. Under these conditions, up-regulation of cell growth and increased focus formation were observed, suggesting an important role of *HERC2* in proliferation [32]. In agreement with these observations, an association of frameshift mutations of *HERC2* with gastric and colorectal carcinoma has been described [18]. Despite the critical role of *HERC2* in cellular processes regulated by p53, little is known about its physiological relevance. The mutation of *HERC2* found among the Old Order Amish with features similar to Angelman syndrome also suggests an important role for *HERC2* in neurodevelopment [4, 5]. To determine the physiological importance of *HERC2*, we decided to generate a mouse with targeted inactivation of the *Herc2* gene.

RESULTS

Characterization of the *Herc2*⁵³⁰ mice

To study the physiological role of HERC2, we generated a novel mutant allele at the *Herc2* locus by

using a gene trapped embryonic stem (ES) cell line from The Sanger Institute. These ES cells, here called *Herc2*⁵³⁰, contain a pGT01xr expression vector with a strong splice acceptor site integrated within intron 2 of the mouse *Herc2* gene, which results in the expression of a truncated mRNA. PCR experiments with genomic DNA from the tails of mice generated with these ES cells confirmed the integration of the trap between exon 2 and 3 (Figure 1A).

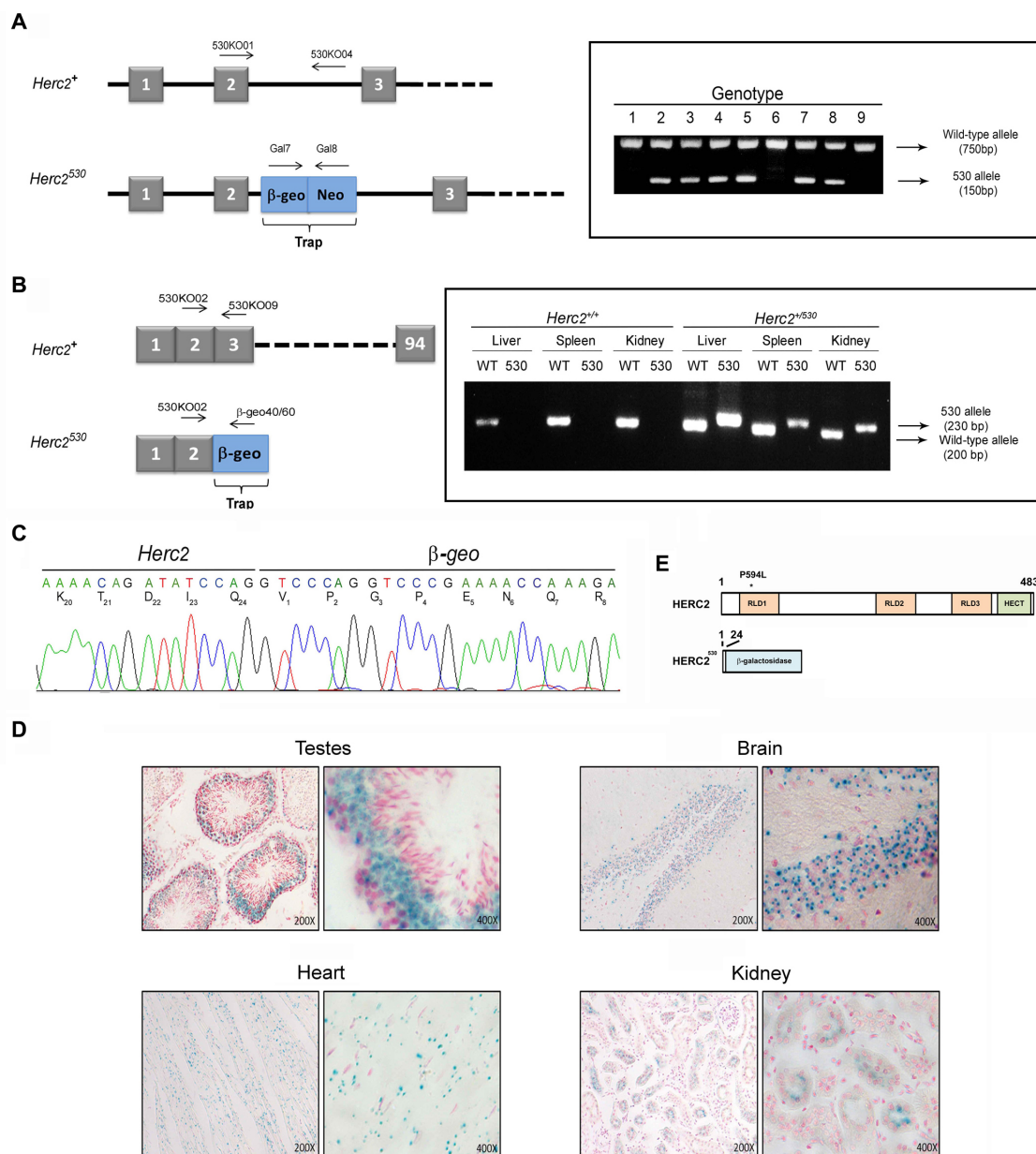


Figure 1: Generation of the *Herc2*⁵³⁰ mice. **A.** Schematic representation of the *Herc2* wild-type allele (*Herc2*⁺) and *Herc2*⁵³⁰ allele and the designed primers to identify both alleles (left). The *Herc2*⁵³⁰ allele contains the pGT01xr vector that expresses the fusion of β -galactosidase and neomycin transferase within intron 2. The integration of the trap was determined by genotyping using the indicated primers (right), 530KO01/530KO04 for the wild-type allele and Gal7/Gal8 for the 530 allele. **B.** Exon structure of *Herc2*⁺ and *Herc2*⁵³⁰ (left). RT-PCR experiments with mRNA from liver, spleen and kidney of *Herc2*⁺ and *Herc2*⁵³⁰ mice was performed using the indicated primers. **C.** PCR products from B were sequenced. The trap was inserted after exon 2, for which the mutant protein contains the first 24 amino acids of the HERC2 and β -galactosidase protein. **D.** β -galactosidase expression in *Herc2*⁵³⁰ mice. The activity of β -galactosidase was determined in the testes, brain, heart and kidney of *Herc2*⁵³⁰ mice and detected by *X-gal* staining. **E.** Scheme of HERC2 protein and the expected product from the *Herc2*⁵³⁰ allele. The P594L pathological mutation is indicated (*). RLD: RCC1-like domain.

RT-PCR experiments with mRNA from different tissues showed the formation of a truncated mRNA of *Herc2* fused to β -galactosidase (β -geo) (Figure 1B). Sequencing analysis confirmed these results and revealed the fusion of β -galactosidase after amino acid residue 24 of HERC2 (Figure 1C). β -galactosidase activity was determined in several tissues (Figure 1D), confirming the expression of a fused transcript of the first 24 amino acid residues of HERC2 with β -galactosidase. Because mouse HERC2 protein has 4,836 amino acid residues, we can consider

that the HERC2 new mutant allele *Herc2*⁵³⁰ is functionally deleted (Figure 1E).

***Herc2* is an essential gene during embryonic development**

91 offspring born from the intercross heterozygous mice were genotyped by PCR. Among these mice, 34 (37%) were wild-type for *Herc2*, and 57 (63%) were heterozygous for *Herc2*⁺⁵³⁰ (Figure 2A). We could not

A

Analysis of mice from a <i>Herc2</i> ^{+/+} × <i>Herc2</i> ⁺⁵³⁰ cross		
Variable	Expected frequency, % (n)	Observed frequency, % (n)
<i>Herc2</i> ^{+/+}	25 (23/91)	37 (34/91)
<i>Herc2</i> ⁺⁵³⁰	50 (45/91)	63 (57/91)
<i>Herc2</i> ^{530/530}	25 (23/91)	0/91

B

Stage	Observed placentas	Placentas with embryo	Placentas without embryo	Genotypes		
				<i>Herc2</i> ^{+/+}	<i>Herc2</i> ⁺⁵³⁰	<i>Herc2</i> ^{530/530}
				E10.5	8	5
E8.5	11	8	3	1	7	0
E7.5	15	7	8	4	3	0

C

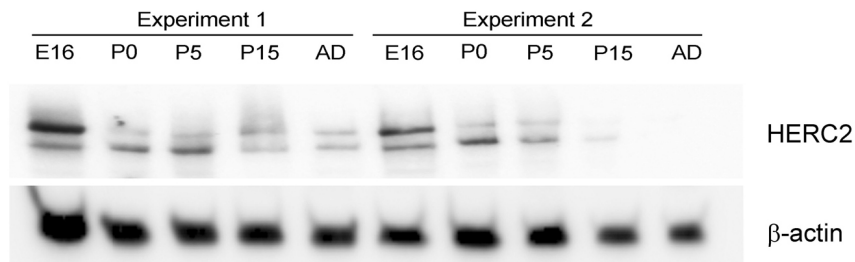


Figure 2: Analysis of progeny from the *Herc2*⁺⁵³⁰ cross. **A.** Analysis of offspring born from the intercross of *Herc2*⁺⁵³⁰ mice. Ninety-one animals were genotyped by PCR of genomic DNA isolated from mouse tails. The expected frequencies for *Herc2*^{+/+} and *Herc2*⁺⁵³⁰ were obtained; however, no homozygous mice (*Herc2*^{530/530}) were identified. **B.** Analysis of embryonic lethality in *Herc2*^{530/530} mice. Embryos from *Herc2*⁺⁵³⁰ pregnant females at different stages were isolated and genotyped. The *Herc2*^{+/+} and *Herc2*⁺⁵³⁰ genotypes were identified, but not the *Herc2*^{530/530}. The placentas without embryos could not be genotyped. **C.** Analysis of HERC2 protein levels during development. Lysates from brains at different stages were analyzed by immunoblotting for HERC2 and β -actin. E16 (embryonic day), P0, P5 and P15 (post-natal day 0, 5 and 15, respectively) and AD (adult animal).

identify any viable homozygous *Herc2*^{530/530}. These data suggested an embryonic lethality for null mice. To determine the time of embryonic lethality in *Herc2*^{530/530} mice, genomic DNA was isolated from embryos harvested at different stages (E7.5, E8.5 and E10.5) of pregnancy from *Herc2*⁺⁵³⁰ mice. We isolated 34 placentas and observed 14 (41%) without embryos (Figure 2B). Among the embryos, we identified both wild-type and heterozygous mice, but not homozygous mice. At day 7.5 and 8.5 in placentas without embryos, we observed some residuals. At day 10.5, these residuals were completely resorbed. Most likely, these residuals were rests of embryos homozygous for *Herc2*⁵³⁰. These results indicate that the expression of at least a normal *Herc2* copy is essential for the completion of embryonic development before day 7.5.

Genes important for development are usually highly expressed during embryonic stages. To determine the expression pattern of the HERC2 protein during

development, we analyzed the levels of the endogenous protein in samples from brains at embryonic day E16, postnatal days P1, P5 and P15, and adult mice (8 weeks). Anti-HERC2 antibodies detected a double band that decreased during development, with the highest levels in the embryonic stage and lower levels in the adult animal (Figure 2C). Similar expression profiles were observed for other members of the HERC family, such as HERC1 or HERC3 (data not shown), suggesting an important role of the HERC proteins during embryonic development.

***p53* inactivation did not rescue embryonic lethality of homozygous *Herc2*⁵³⁰ mice**

Growth curves and survival rates were analyzed in *Herc2*⁺⁵³⁰ mice. The growth curve was not significantly altered in *Herc2*⁺⁵³⁰ mice during the time studied (Figure 3A). The survival rate was also similar to wild-type mice during the period studied (Figure 3B).

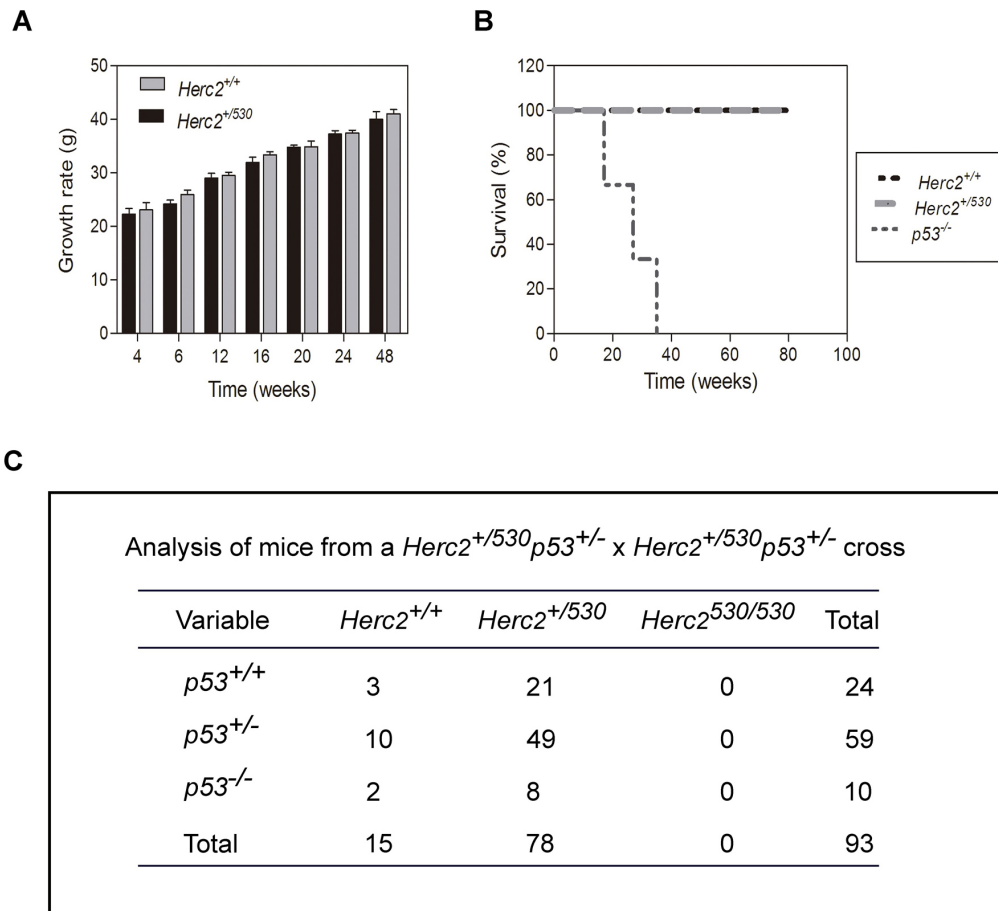


Figure 3: *p53* inactivation did not rescue the lethality of *Herc2*^{530/530} homozygous mice. Graphs of growth rate **A**, and survival **B**, from *Herc2*^{+/+} and *Herc2*⁺⁵³⁰ mice. Growth and survival were analyzed in male mice (n>10) at the indicated weeks. The survival for *p53*^{-/-} mice also was analyzed. **C**. The analysis of mice from a cross of double heterozygous *Herc2*⁺⁵³⁰ *p53*^{+/-} animals. The offspring was genotyped by PCR of genomic DNA with the appropriate primers, indicating that the embryonic lethal phenotype of *Herc2*^{530/530} embryos was not rescued by crossing with *p53*^{-/-} mice.

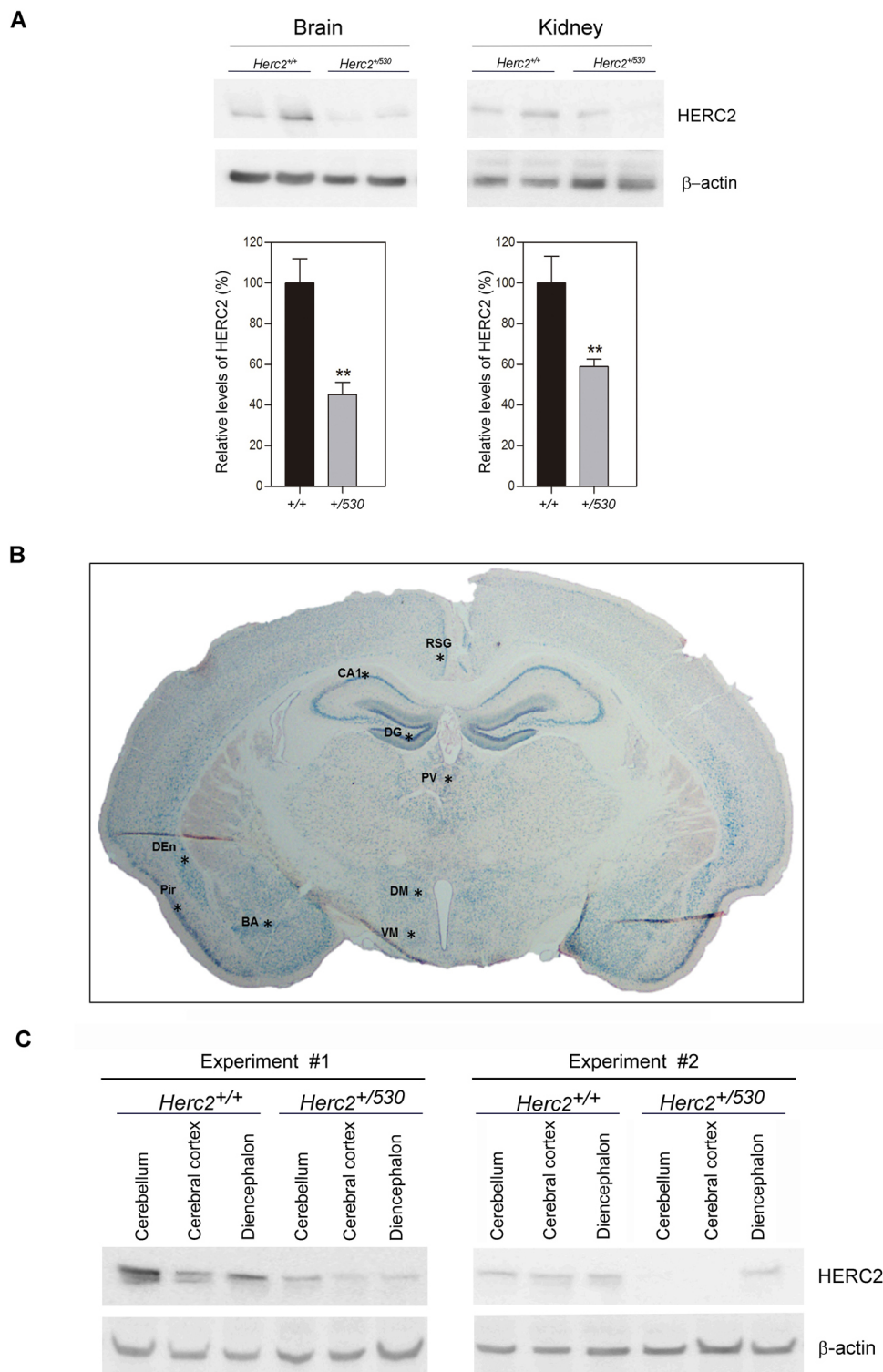


Figure 4: *Herc2*⁺⁵³⁰ mice show reduced levels of HERC2 protein. **A.** HERC2 protein levels were analyzed by immunoblotting using specific antibodies against HERC2 in several tissues from 8 week old mice. The levels of HERC2 were quantified ($n = 8$) and normalized with respect to β -actin levels. **B.** β -galactosidase expression in brain from *Herc2*⁵³⁰ mouse. The β -galactosidase activity was detected ubiquitously in all areas using *X-gal* staining. However, there were forebrain cortical and subcortical areas in which β -galactosidase labeling was the most intense (asterisks). **C.** The levels of HERC2 were analyzed by immunoblotting in lysates of cerebellum, cerebral cortex and diencephalon from *Herc2*^{+/+} and *Herc2*⁺⁵³⁰ mice at P4 (post-natal day 4). BA, basal amygdala. CA1, pyramidal cell layer of the hippocampal cornu ammonis 1. DEn, dorsal endopiriform nucleus. DG, granular cell layer of hippocampal dentate gyrus. DM, dorsomedial nucleus of the hypothalamus. Pir, piriform cortex. PV, paraventricular thalamic nucleus. RSG, retrosplenial granular cortex. VM, ventromedial nucleus of the hypothalamus.

It had been previously demonstrated that knockout mice for the E3 ubiquitin ligases of p53, such as *MDM2* or *MDM4*, are lethal in embryonic stages due to growth inhibition and apoptosis. Interestingly, this lethality could be rescued by concomitant p53 depletion [33-35]. Because HERC2 is an E3 ubiquitin ligase that regulates p53 activity [32], we asked whether p53 inactivation might also rescue the lethality of *Herc2^{530/530}* homozygous mice. We crossed double heterozygous *Herc2* and *p53* mice (*Herc2^{+/-530} p53^{+/-}* mice) to obtain double homozygous mice. We analyzed the genotype of the offspring by performing an adequate PCR assay on of genomic DNA samples but did not observe any viable *Herc2^{530/530}* mouse (Figure 3C). These data suggest the non-involvement of p53 in the embryonic death caused by the depletion of *Herc2*.

Partial inactivation of the *Herc2* gene is sufficient to reduce HERC2 protein levels and activity

We analyzed protein levels of HERC2 in *Herc2^{+/-530}* animals by immunoblotting. We observed that the levels of HERC2 were decreased approximately 50% in the brain and kidney of *Herc2^{+/-530}* animals (Figure 4A). The analysis of β -galactosidase activity in *Herc2^{+/-530}* mice allows the analysis of *Herc2* expression in more detail. Ubiquitous expression of HERC2 was observed in all tissues analyzed (Figure 1D). In the brain, this expression was higher in the hippocampus (pyramidal cell layer and granular layer of dentate gyrus), hypothalamic nucleus (dorsomedial and ventromedial), amygdaloid nucleus (basal and medial), piriform cortex, dorsal endopiriform nucleus, entorhinal cortex, retrosplenial cortex, paraventricular thalamic nucleus, and cerebellum (Figure 4B and data not shown).

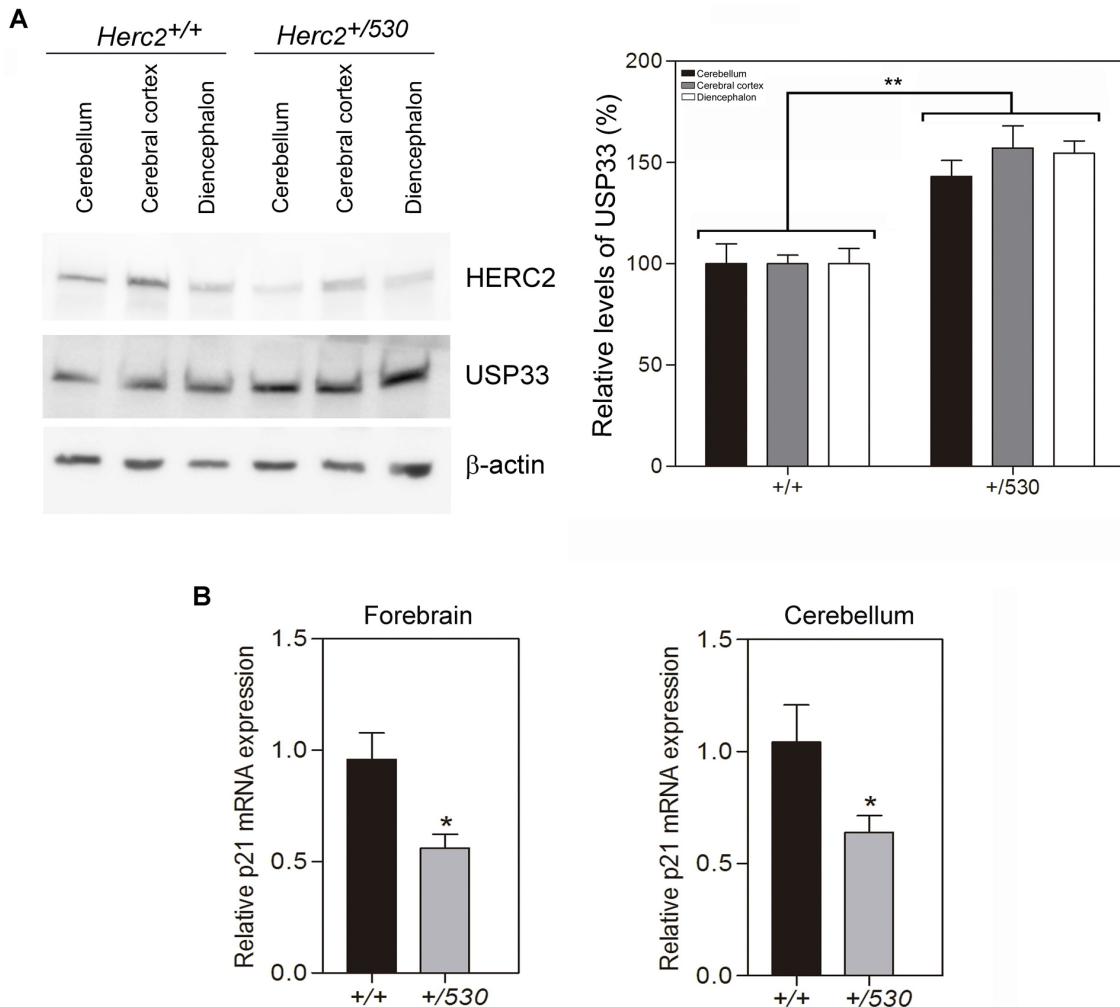


Figure 5: *Herc2^{+/-530}* mice show reduced activity of HERC2. **A.** USP33, a substrate of ubiquitination of HERC2, was analyzed in lysates (cerebellum, cerebral cortex and diencephalon) from 8 week old mice by immunoblotting. Higher levels of USP33 were observed in all areas of *Herc2^{+/-530}* mice. Levels of USP33 were quantified and normalized with respect to β -actin levels. **B.** *Herc2^{+/-530}* mice show reduced levels of *p21* mRNA. RT quantitative PCR analyses were performed in forebrain and cerebellum from *Herc2^{+/+}* and *Herc2^{+/-530}* mice to quantify *p21* gene expression ($n = 10$). The levels of expression were normalized with respect to *GAPDH* gene expression.

Table 1: Behavioural tests of *Herc2*^{+/⁵³⁰ mice}

Cognitive task	Behavioural tests		Test Values: mean ± error (n)		P value
			<i>Herc2</i> ^{+/⁺}	<i>Herc2</i> ^{+/⁵³⁰}	
Anxiety	Time outside of the dark box (s)		235 ± 13 (9)	232 ± 9 (8)	0.83
	Immobile time suspended by the tail (s)		205 ± 14 (9)	173 ± 14 (19)	0.11
Learning and Memory	Object recognition memory (DI)	STM	0.24 ± 0.08 (6)	0.23 ± 0.05 (10)	0.87
		LTM	0.26 ± 0.09 (6)	0.32 ± 0.06 (10)	0.60
	Step through passive avoidance test (Latency)	STM	2.92 ± 0.24 (6)	2.21 ± 0.37 (15)	0.12
		LTM	2.84 ± 0.31 (7)	3.04 ± 0.32 (19)	0.66
Motor function	Open field (total activity)		1649 ± 108 (8)	1612 ± 199 (16)	0.87
	Rotarod (#Falls)		1.14 ± 0.46 (7)	4.21 ± 0.90 (19)	**0.0058
	Forelimb Grip strength (s)		7.00 ± 0.98 (6)	7.96 ± 0.78 (8)	0.46

STM: Short Term Memory; LTM: Long Term Memory; DI: Discrimination index; n: number of animals

These observations were confirmed by immunoblotting. We dissected the cerebellum, cerebral cortex and diencephalon, detecting HERC2 protein in all these areas (Figure 4C). The levels of HERC2 protein were reduced in *Herc2*^{+/⁵³⁰ animals (Figure 4C) with respect to control mice (*Herc2*^{+/⁺).}}

These data show that the levels of HERC2 protein are reduced almost 50% in *Herc2*^{+/⁵³⁰ mice tissues and suggest that the HERC2 activity must also decrease in the brain of heterozygous animals. Two activities have been associated with HERC2 protein; an E3 ubiquitin ligase activity which regulates protein levels of USP33, BRCA1 or XPA [21, 22, 25], and an activity as a stimulator of the p53 oligomerization that regulates the transcriptional activity of p53 [32]. To analyze the activity of E3 ubiquitin ligase, we performed immunoblotting experiments in the mouse brain areas with antibodies against substrates ubiquitinated by HERC2. Only the USP33 protein was detected by immunoblotting in these mouse samples (Figure 5A). Interestingly, in *Herc2*^{+/⁵³⁰ mice, the levels of USP33 were higher than in control mice. To examine the activity stimulating p53 oligomerization and transcriptional activity, we analyzed the levels of *p21* mRNA by RT quantitative PCR analysis. A decrease in *p21* mRNA levels was observed in *Herc2*^{+/⁵³⁰ mice (Figure 5B). Altogether, these data show that the partial inactivation of the *Herc2* gene in *Herc2*^{+/⁵³⁰ mice is sufficient to reduce HERC2 protein levels and activity.}}}}

A homozygous mutation in human *Herc2* causes an Angelman-like syndrome and reduces the activity of the HERC2 protein

HERC2 has been implicated in a human disorder with some features similar to Angelman syndrome. The substitution of proline by leucine at amino acid position 594 in HERC2 caused HERC2^{P594L} instability and almost

total loss of the protein in homozygosis [4, 5]. Based on our data from heterozygous animals, we hypothesized that these patients would have lower levels of HERC2 activity. To test this hypothesis, we analyzed the levels of USP33 protein from fibroblasts derived from an affected individual and a healthy control. We observed a high increase of USP33 levels in fibroblasts from a patient (Figure 6A). To confirm that HERC2 activity was diminished, we also analyzed the levels of p21 protein. We observed a decrease in the p21 protein levels in fibroblasts from this patient (Figure 6A). However, the p53 and α -tubulin levels did not significantly change. The *p21* mRNA levels also confirmed the decrease in p53 transcriptional activity in fibroblasts from the patient (Figure 6B). The level of p53 protein is regulated by the proteasome. In the presence of the proteasome inhibitor MG132, we observed a similar stabilization of p53 protein levels in fibroblasts from the patient and the control (Figure 6C). Under these conditions, we also detected a decrease in p21 protein levels in fibroblasts from the patient (Figure 6C), indicating a decrease in its p53 activity. These data show the low activity of HERC2 in individuals carrying the HERC2^{P594L} mutation.

In conclusion, the low HERC2 activity found in *Herc2*^{+/⁵³⁰ mice (Figure 5) and in individuals with the HERC2^{P594L} mutation (Figure 6A-6C) correlated with an increase in levels of the USP33 protein and a decrease in levels of the p21 protein. These data suggest that in conditions with low levels of HERC2 protein, cells could contain more USP33 and less p21. To confirm this point, human U2OS cells were depleted of HERC2 using interference RNA, and USP33 and p21 were analyzed by immunoblotting (Figure 6D). HERC2 knockdown increased levels of the USP33 protein and decreased levels of the p21 protein.}

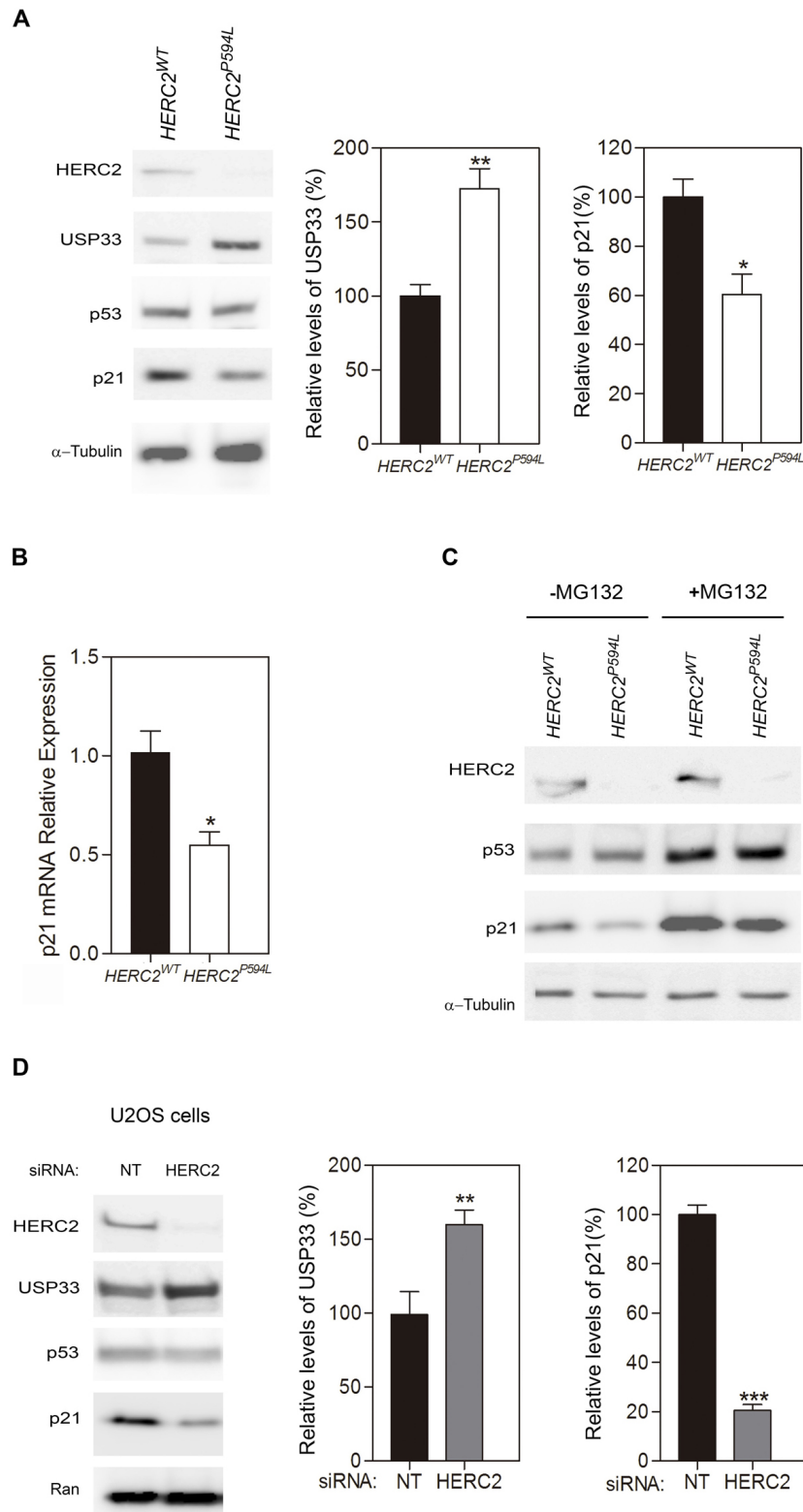


Figure 6: A homozygous mutation in human *HERC2* that causes an Angelman-like syndrome reduces the activity of the *HERC2* protein. **A.** Fibroblasts derived from individuals with *HERC2* wild-type or *HERC2* with the mutation P594L were analyzed by immunoblotting for the indicated antibodies. Levels of USP33 and p21 proteins were quantified and normalized with respect to α -tubulin levels. **B.** Levels of *p21* mRNA were analyzed by RT quantitative PCR analysis and normalized with respect to *18S* gene expression. **C.** The levels of *HERC2*, p53, p21 and α -tubulin proteins were analyzed in the presence or absence of the proteasome inhibitor MG132. **D.** U2OS cells were transfected with non-targeting (NT) or *HERC2* siRNAs and analyzed by immunoblotting against the indicated proteins. The levels of USP33 or p21 were quantified and normalized with respect to Ran levels.

HERC2 regulates motor coordination

Individuals carrying the $HERC2^{P594L}$ mutation present a severe developmental delay with an unstable gait [4,5]. We wondered whether $Herc2^{+/530}$ mice with

a reduction of approximately 50% in $HERC2$ protein could have some features found in $HERC2^{P594L}$ patients. To examine this question, behavioural tests to measure different cognitive tasks were performed in $Herc2^{+/530}$ and wild-type mice. Except for the rotarod test, no significant

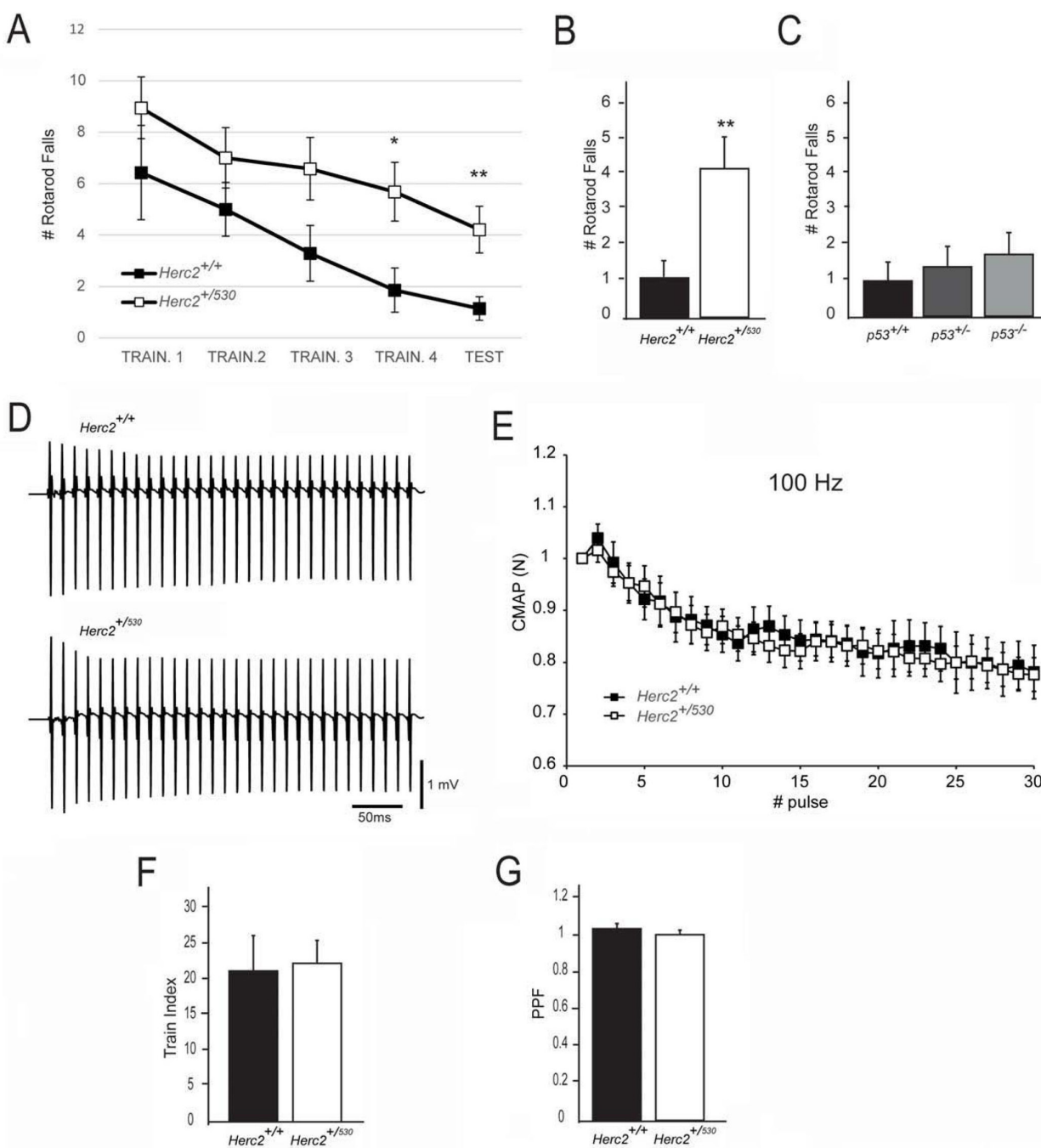


Figure 7: Impaired motor coordination in $Herc2^{+/530}$ mice. A-B. The number of falls from the rotarod increases in $Herc2^{+/530}$ mice at 6 months of age in comparison with control littermates. C. No difference was found in $p53^{+/-}$ and $p53^{-/-}$ mice in comparison with WT. (D-E) EMG measurements of CMAP amplitudes in the MG of control and $Herc2^{+/530}$ mice show normal neurotransmission efficacy in postnatal heterozygous mice. D. Representative recordings during a train of stimuli at 100 Hz in a control and a $Herc2^{+/530}$ mouse. E. Depression of CMAP amplitudes (normalized to the first response) during a train of stimuli of 300 ms at 100 Hz in control ($n = 7$) and heterozygous mice ($n = 18$). The train index F., corresponding to the depression at the end of the train, and PPF (Pair -Pulse Facilitation) G., are similar between groups.

differences between the two groups were found (Table 1; Supplementary Video). *Herc2*^{+/⁵³⁰ mice displayed a statistically significant increase in rotarod falls compared to wild-type mice (*Herc2*^{+/⁺: 1.14 ± 0.46, *n* = 7 and *Herc2*^{+/⁵³⁰: 4.21 ± 0.90, *n* = 19, *p* = 0.0058) (Figure 7A-7B), suggesting a role for HERC2 in motor coordination. Because HERC2 regulates p53 activity, we asked whether p53 inactivation could produce effects similar to *Herc2*^{+/⁵³⁰ mice. We performed the rotarod test in *p53*^{+/⁻ and *p53*^{-/⁻ mice. No significant differences were observed compared to wild-type mice (Figure 7C). These data indicate that the impaired motor coordination in *Herc2*^{+/⁵³⁰ mice is specific and independent of p53. Next, we analyzed whether muscular function was affected in *Herc2*^{+/⁵³⁰ mice. The electrical neuromuscular properties of the *Herc2*^{+/⁵³⁰ mice were studied *in vivo* by performing electromyography (EMG) on the medial gastrocnemius (MG) muscle using short train stimuli at 100 Hz (Figure 7D). The depression at the end and the facilitation at the beginning of a train of 30 stimuli were similar in mutant and wild-type mice when measured by normalization of the CMAP (Compound Muscular Action Potentials) amplitude (*p* = 0.8 and *p* = 0.85, respectively) (Figure 7E-7G). These results indicate a normal muscular function.}}}}}}}}}

The cerebellum regulates motor coordination, and alterations in its structure have been associated with impaired motor coordination. To examine whether the deficit of motor synchronization in *Herc2*^{+/⁵³⁰ mice was caused by an alteration of cerebellar structure, we performed immunohistochemistry analysis of the specific marker of Purkinje cells calbindin-D28 k (CaBP) (Figure 8). CaBP immunoreactive Purkinje cell somata form a continuous cell layer in the cerebellar cortex of *Herc2*^{+/⁺ mice (Figure 8A-8C). In *Herc2*^{+/⁵³⁰ mice, parasagittal zones devoid of immunoreactivity throughout the cerebellum indicative of Purkinje cell loss were observed (arrows and arrowheads in Figure 8D-8F). These symmetrical Purkinje cell-deprived bands -characterized by the presence of wide spaces lacking cell somata in the Purkinje cells layer (asterisks in Figure 8H) and dendritic debris through the molecular layer (mol in Figure 8H)-, were distributed differently along a medio-lateral gradient (see comparison between Figure 8D-8F from a *Herc2*^{+/⁵³⁰ mouse and Figure 8A-8C from a *Herc2*^{+/⁺ mouse). Thus, vermal and paravermal Purkinje cells were less affected than in the cerebellar hemispheres. In the vermis and paravermis, the loss of Purkinje cells was distributed in narrow gaps (arrows in Figure 8D and 8E), while at the hemispheres, the areas of Purkinje cells loss reached a great extension (arrowheads in Figure 8D and 8F), in which remain some surviving Purkinje cells (small arrows in Figure 8F). Epifluorescence microscopy analysis showed that HERC2 immunoreactivity in Purkinje cells colocalize with CaBP (Figure 9). In *Herc2*^{+/⁵³⁰ mice, HERC2 immunohistochemistry confirmed the loss of}}}}}}

Purkinje cells in narrow gaps at the vermis/paravermis or in a greater extension at the hemispheres (Figure 9C-9E).

CaBP immunohistochemistry also revealed the presence of pathological signs in *Herc2*^{+/⁵³⁰ Purkinje cells. Rounded thickenings resembling axonal torpedoes were observed in Purkinje cell axons, which contrast with the fine grained morphology of normal Purkinje cells axonal plexuses (see arrows in the comparison between *Herc2*^{+/⁺ and *Herc2*^{+/⁵³⁰ in Figure 10A-10C). Phenotypic alterations of *Herc2*^{+/⁵³⁰ Purkinje cells were also observed in the 1.5 μm thick sections stained with toluidine blue (Figure 10D-10E). Disappeared Purkinje cells somata were substituted by glial Golgi-epithelial cells (Figure 10D: arrows, Purkinje cells; small arrows, Golgi-epithelial cells). High magnification allowed to detect degenerative dark accumulations within the cytoplasm of the soma (arrowheads in Figure 10E) and the dendrites (arrows in Figure 10E) of the Purkinje cells. Electron microscopy analysis of cerebella confirmed these degenerative signs in *Herc2*^{+/⁵³⁰ mice (Figure 10F-10H and 11). The cytoplasm of *Herc2*^{+/⁵³⁰ Purkinje cells contained a high number of lysosomes and electron-dense debris (Figure 10F-10H, asterisks), and autophagosomes with different degrees of evolution (Figure 10G, arrows). Damaged cisterns of Golgi apparatus and numerous cisterns of the rough endoplasmic reticulum fused to the cytoplasmic face of the nuclear membrane were also observed (not shown). The difference between mice *Herc2*^{+/⁺ and *Herc2*^{+/⁵³⁰ was even most evident in the principal Purkinje cell dendrites (Pcd in Figure 11). Thus, numerous degenerative signs were present in *Herc2*^{+/⁵³⁰ Purkinje cells dendrite (Figure 11B and 11E), while were almost absent in wild-type ones (Figure 11A, 11C and 11D). These degenerative signs were found in 2 and 9 month-old animals (Figure 10F-10H), with a slight increase of these alterations in the older mice (not shown). These data show that the partial inactivation of HERC2 in *Herc2*^{+/⁵³⁰ mice causes Purkinje cell loss, which explain motor incoordination detected here in rotarod test. The increase of autophagosomes and lysosomes observed in *Herc2*^{+/⁵³⁰ Purkinje cells (Figure 10 and 11) led us to wonder whether HERC2 may be involved in the regulation of autophagy. To this end, we have analyzed the adaptor-substrate p62/SQSTM1 by laser confocal microscopy. HERC2 immunostaining colocalized with p62 (Figure 12). This colocalization, it was observed both in wild-type animals as in *Herc2*^{+/⁵³⁰ animals (Figure 12, arrows and arrowheads in the merged). In *Herc2*^{+/⁺ mice, p62 immunostaining showed a punctate labeling pattern that concentrated in Purkinje cells somata (Figure 12, arrows). This pattern was altered in *Herc2*^{+/⁵³⁰ animals; thus, in addition to the somatic labeling, p62 immunostaining was also evident within the dendritic trees and the axonal torpedoes of Purkinje cells (Figure 12, arrows and arrowheads) indicating a dysregulation of autophagy in *Herc2*^{+/⁵³⁰ Purkinje cells. Altogether,}}}}}}}}}}}}}}}

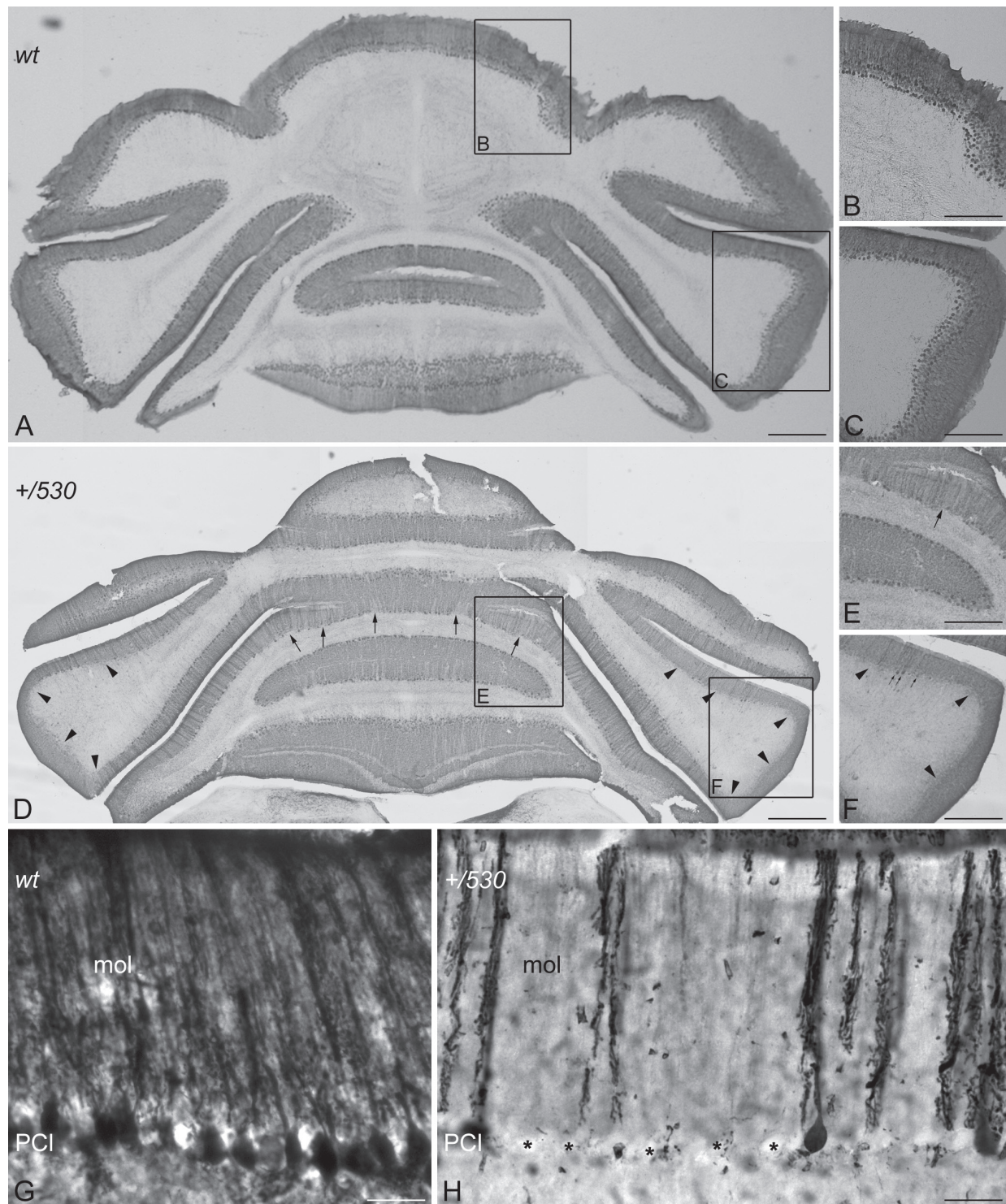


Figure 8: Purkinje cells loss in *Herc2*⁺⁵³⁰ mice. Microphotographs of coronal sections through the cerebellar cortex of 9 months old wild-type (*wt*, A-C, G) and 9 months old *Herc2*⁺⁵³⁰ mice (+/530, D-F, H). Calbindin immunohistochemistry shows as Purkinje cell somata form a continuous cell layer in the *Herc2*⁺⁵³⁰ (*wt*) cerebellum (A-C) However, parasagittal zones lacking of immunoreactivity throughout the *Herc2*⁺⁵³⁰ cerebellum indicative of Purkinje cell loss are observed (arrows and arrowheads, in (D-F)). These symmetrical Purkinje cells deprived bands, characterized by the presence of wide spaces lacking Purkinje cell somata (H, asterisks) and dendritic debris through the molecular layer (H, mol), distribute differently according a medio-lateral gradient. In the vermis and paravermal zones the immunonegative zones are sagittally distributed in narrow gaps (D-E, arrows); while at the hemispheres the areas devoid of Purkinje cells, also bilateral, reach a greater extension (D, F, arrowheads) in which remain some surviving Purkinje cells (F, small arrows). G, illustrates the *Herc2*⁺⁵³⁰ (*wt*) immunostaining of normal Purkinje cells; note as dendritic trees fulfill the molecular layer (G, mol), while Purkinje cells somata align in a continuous row. PCI, Purkinje cells layer. Bars = 600 μ m (A, D), 400 μ m (B-C, E-F), and 30 μ m (G-H).

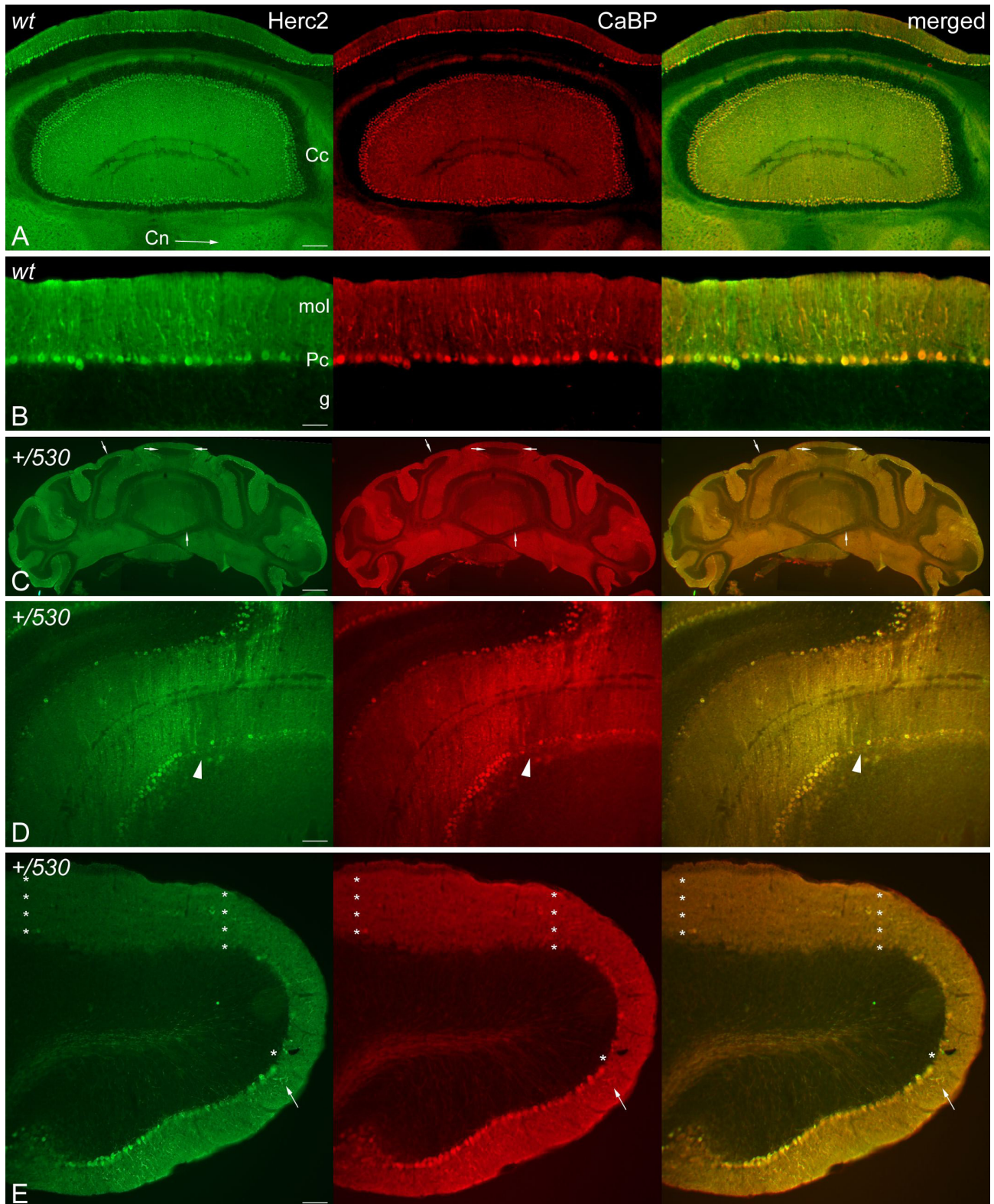


Figure 9: HERC2 is present in Purkinje cells. Microphotographs of coronal sections through the cerebellar cortex of 9 months old *Herc2*^{+/+} (wt, A.-B.) and 9 months old *Herc2*⁺⁵³⁰ mice (+/530, D.-E.). Epifluorescence microscopy analysis shows that HERC2 is expressed in all the adult Purkinje cells colocalizing with the general marker of Purkinje cell calbindin (CaBP) (A-E) in the cerebellar cortex (A, Cc), and their axonal endings in the cerebellar nuclei (A, Cn, arrow). *Herc2*⁺⁵³⁰ cerebellum displays parasagittal bands of Purkinje cells loss in the vermis and paravermal zones (C., arrows; D, arrowheads), and areas of extensive Purkinje cell loss in the cerebellar paraflocculus (asterisks). The arrows in E illustrate the co-expression of both proteins in the Purkinje cell dendritic tree. Bars = 750 μ m (C), 200 μ m (A), 100 μ m (D), 75 μ m (E), and 50 μ m (B).

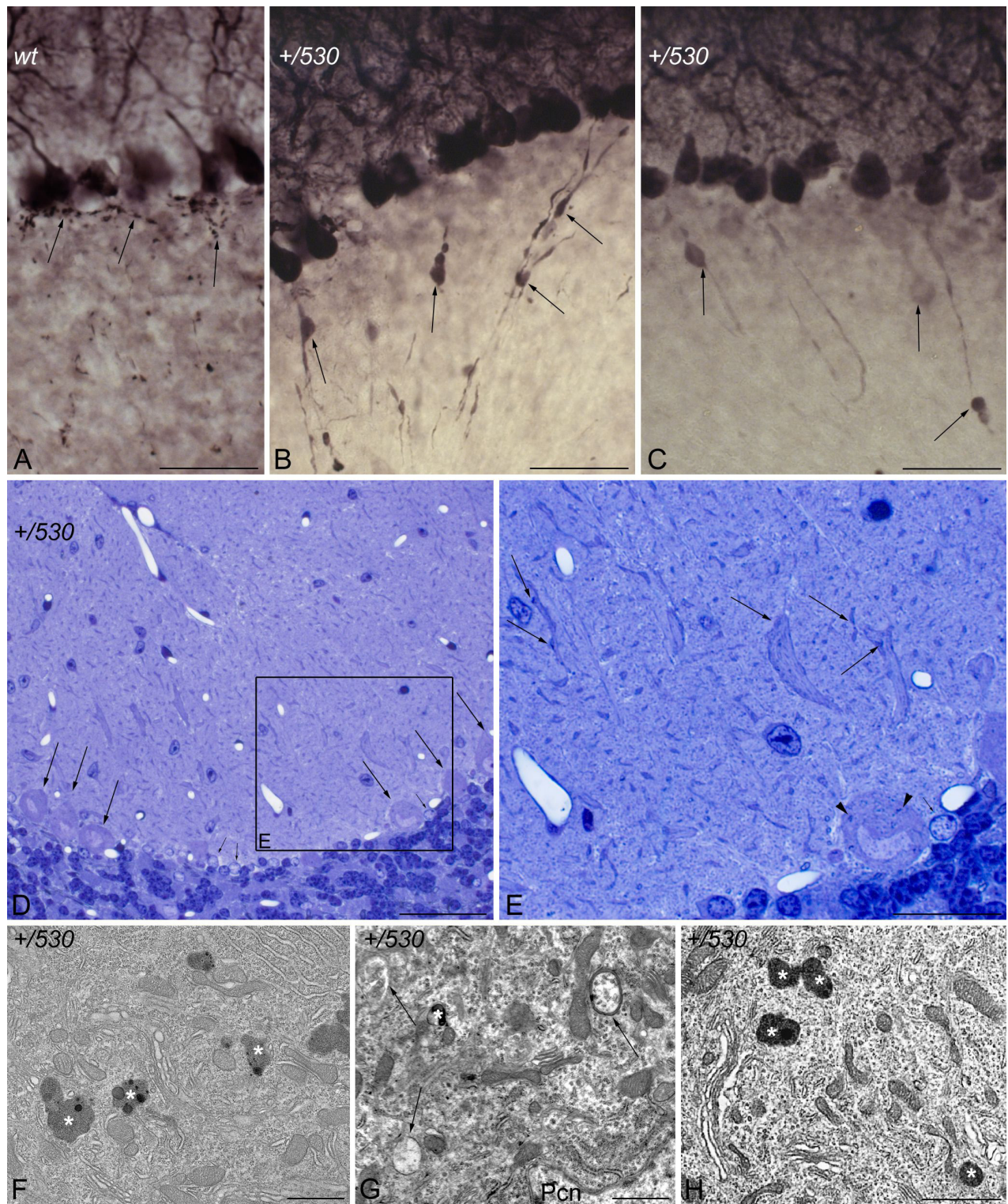


Figure 10: Purkinje cell degeneration in *Herc2*⁺⁵³⁰ mice. Microphotographs of transmitted light A.-E. and electron microscopy F.-H. of parasagittal sections through the cerebellar cortex of 9 months *Herc2*^{+/+} (wt, A), and 2 (H) and 9 months old *Herc2*⁺⁵³⁰ mice (+/530, B.-G.). Calbindin immunohistochemistry reveals the presence of rounded thickenings resembling to axonal torpedoes in *Herc2*⁺⁵³⁰ Purkinje cell axons (B-C, arrows), which contrast with the fine grained morphology of normal Purkinje cells axonal plexuses (A, arrows). 1.5 μm thick sections illustrated Purkinje cells (D, arrows) limiting a zone in which disappeared Purkinje cells were substituted by glial Golgi-epithelial cells (small arrows in D and E). High magnification allows detect degenerative dark accumulations within the cytoplasm of the soma (E, arrowhead) and the dendrites (E, arrows) of the Purkinje cells. *Herc2*⁺⁵³⁰ Purkinje cells cytoplasm possesses lysosomes, electron-dense debris (F-H, asterisks), and autophagosomes with different degrees of evolution (G, arrows). Pcn, Purkinje cell nucleus. Bars = 50 μm (A-D), 25 μm (E), and 1 μm (F-H).

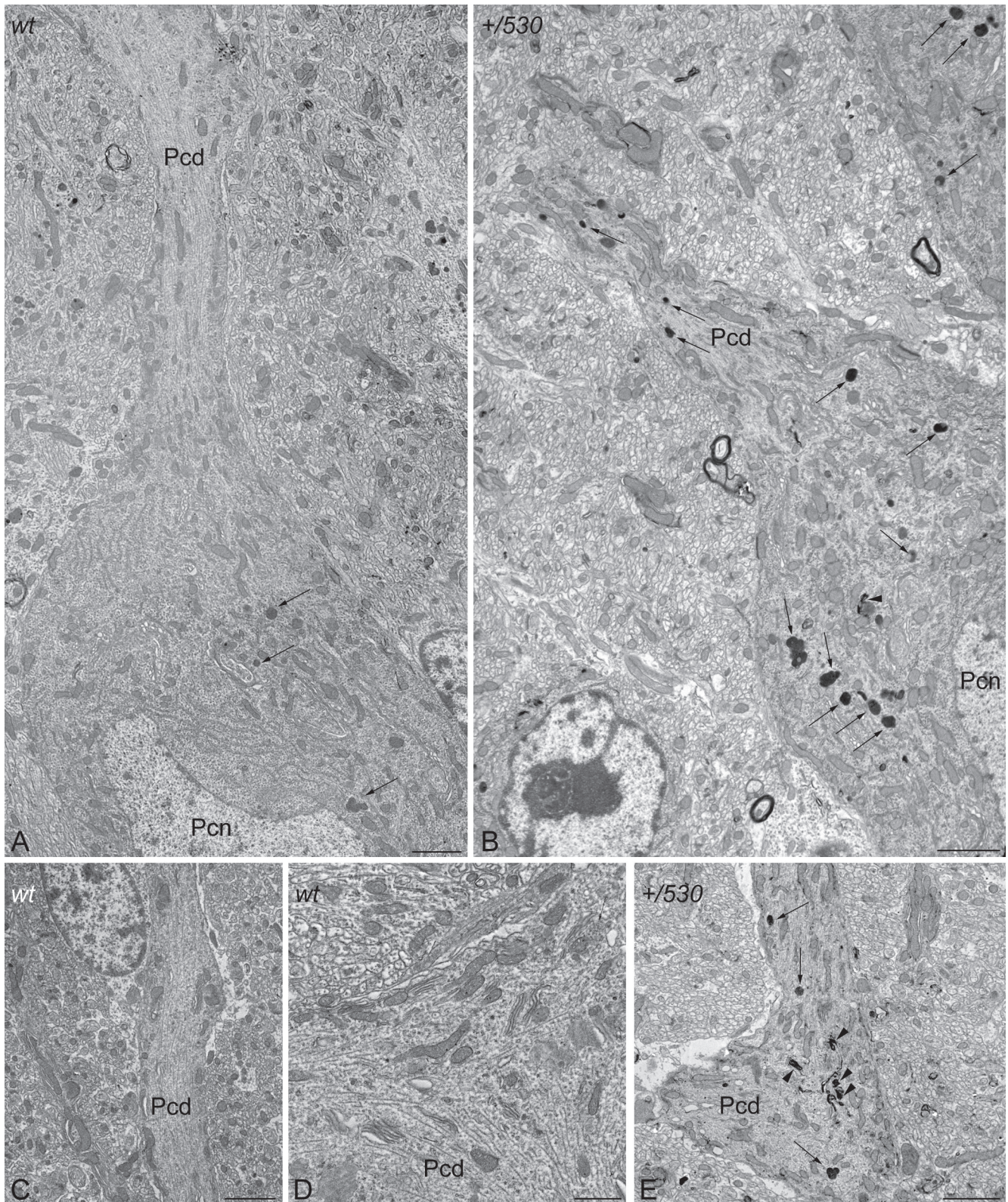


Figure 11: Ultrastructural analysis of *Herc2*⁺⁵³⁰ mice indicates accumulation of autophagosomes and lysosomes in Purkinje cells. Electron photomicrographs of parasagittal sections through the cerebellar vermis of 9 months old *Herc2*^{+/+} (wt, A, C-D.) and 9 months old *Herc2*⁺⁵³⁰ mice (+/530, B, E.). An important difference in the presence of autophagic (arrowheads), and lysosomal (arrows) organelles can be observed between wild-type (A) and *Herc2*⁺⁵³⁰ (B) Purkinje cells cytoplasm. The difference is even most evident in the principal Purkinje cell dendrites. Thus, numerous degenerative signs are present in *Herc2*⁺⁵³⁰ Purkinje cells dendrite (E), while are almost absent in wild-type ones (C-D). Pcd, Purkinje cell dendrite. Pcn, Purkinje cell nucleus. Bars = 2 μ m (A-C, E), and 1 μ m (D).

these findings suggest that HERC2 plays an active role in regulating the Purkinje cells homeostasis, whose deregulation elicits alterations in motor coordination.

DISCUSSION

We have generated a new mutant allele of the HERC2 ubiquitin ligase, *Herc2*⁵³⁰, which has led us to identify *Herc2* as an essential gene for embryonic development. The *HERC2* gene encodes an unusual long polypeptide chain of almost 5,000 amino acid residues. The maintenance during evolution of this single and long polypeptide chain suggests an important physiological role for the giant HERC2 protein. Here, we showed that the inactivation of *Herc2* causes embryonic lethality before 7.5 days. At that time, we observed a high number of abnormal placentas, probably indicating resorption of unviable embryos. Although we have not studied the cause of this embryonic lethality, a possibility could be defective implantation. The unviability of embryos when HERC2 is inactivated would be indicative of the difficulty of finding human individuals homozygous for mutations of this gene.

To our knowledge, only the HERC2^{P594L} mutation found in the Amish community has been reported in humans [45]. In these individuals, the HERC2 protein is unstable and low levels are detected, although apparently high enough to avoid embryonic lethality. Ubiquitin ligases that interact with p53, such as MDM2 or MDM4, had also been identified as essential during embryonic phases. The absence of MDM2 induces embryonic lethality in mice at the peri-implantation (E4-E5.5) stage of development, whereas mice deficient for MDM4 die in mid-gestation (E7.5-E8.5) [33-35]. The lethality during these phases was rescued by a double knockout of the ubiquitin ligase and p53 [33-35]. Because HERC2 is also an ubiquitin ligase that interacts and regulates p53 activity [32], we analyzed whether the double knockout of HERC2 and p53 could also rescue the lethality. Our results show that the double knockout did not rescue the embryonic lethality, indicating a p53-independent role for HERC2 in development. Moreover, these data also confirm, at a genetic level, the different functions of MDM2 (or MDM4) and HERC2 in p53 regulation.

HERC2 acts as an ubiquitin ligase tagging for degradation by the proteasome of substrates such as XPA,

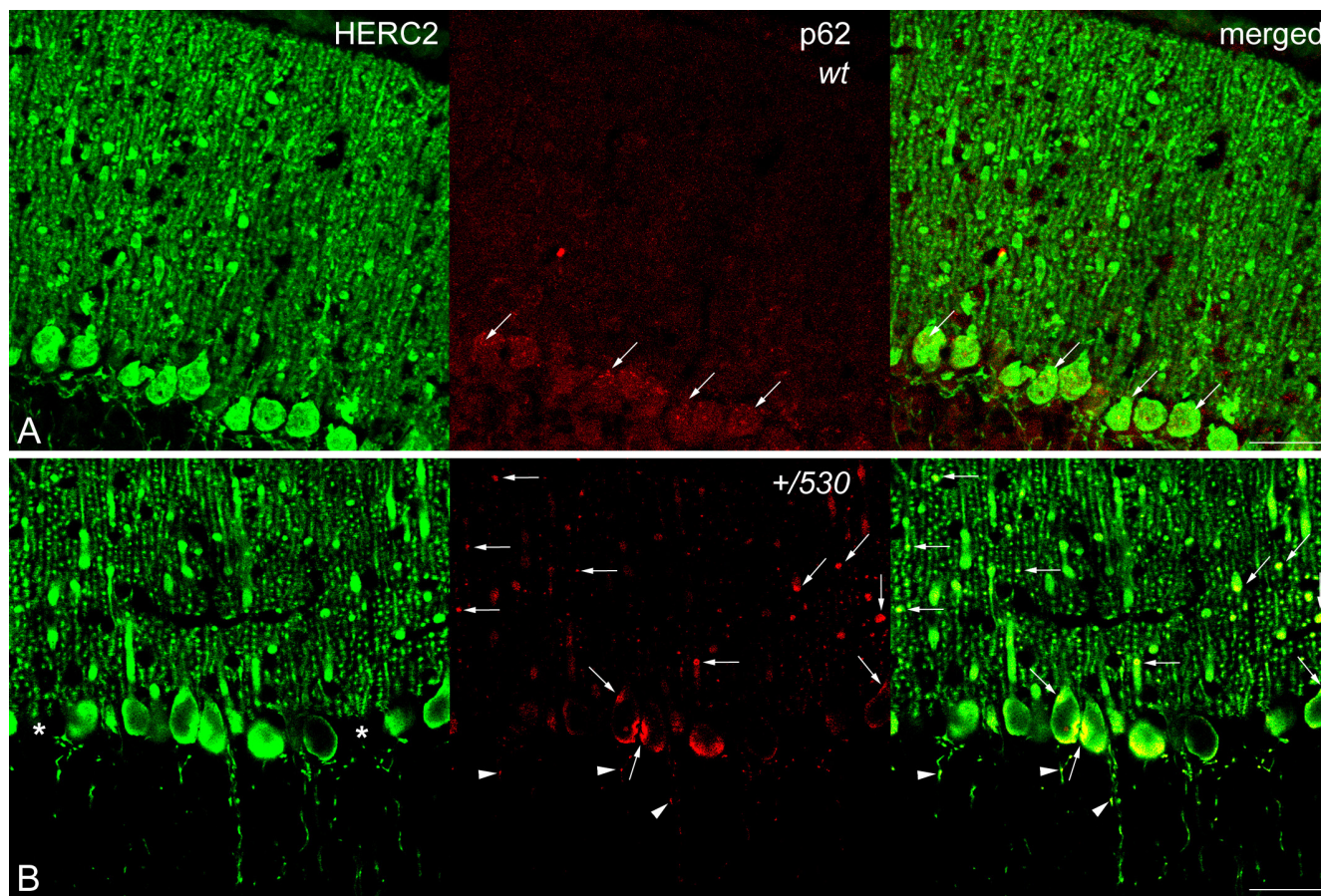


Figure 12: p62/SQSTM1 in *Herc2*⁺⁵³⁰ mice. Laser confocal microphotographs of coronal sections through the cerebellar cortex of the vermis of 9 months *Herc2*^{+/+} (*wt*, A) and 9 months old *Herc2*⁺⁵³⁰ (*+530*, B) mice double labeled with HERC2 and p62 antibodies. Colocalizations of HERC2 and p62 are indicated by arrows in dendrites and cell somata **A**, **B**, and by arrowheads in the axonal torpedoes of *Herc2*⁺⁵³⁰ Purkinje cells (B). Asterisks in B indicate the absence of Purkinje cell bodies. Bar = 50 μ m (A-B).

BRCA1, NEURL4, FBXL5 or USP33 [21, 22, 24-26]. HERC2 may also positively regulate p53 activity through stimulation of its oligomerization [32]. The analysis of levels of USP33 and p21 led us to analyze these two activities, respectively. These activities had been reported in culture cell but not in physiological conditions. The generation of *Herc2*^{+/⁵³⁰} mice containing approximately one-half of the HERC2 protein (Figure 4) led us to analyze the role of HERC2 *in vivo*. *Herc2*^{+/⁵³⁰} mice had higher levels of USP33 protein and lower levels of p21 mRNA (Figure 5). These results show for the first time the inhibition of HERC2 activity in physiological conditions. Individuals from the Amish community with a punctual mutation in HERC2, HERC2^{P594L}, suffer a developmental disorder with features similar to Angelman syndrome [4,5]. These individuals produce an instable HERC2^{P594L} protein. Skin fibroblasts obtained from these individuals also had higher levels of USP33 protein and lower levels of p21, in agreement with a loss of HERC2 activity. We showed how these results can be extrapolated to other human cells through interference RNA experiments. HERC2 knockdown caused an increase in the levels of USP33 protein and a decrease in the levels of p21. In conclusion, we show how the loss of HERC2 protein correlates with the loss of its activities, confirming the involvement of HERC2 in cellular processes regulated by USP33 [25] and p53 [32].

The tumor suppressor gene *p53* is mutated in approximately 50% of human sporadic cancers and in inherited cancer predispositions, such as Li-Fraumeni syndrome [27, 28]. Homozygous *p53*^{-/-} mice are highly prone to cancer, particularly T-cell lymphoma and sarcoma [36, 37]. Experiments with heterozygous *p53*^{+/-} mice indicate that a mere reduction in p53 levels may be sufficient to promote tumorigenesis [38]. The p53 transcriptional activation is dependent of its oligomerization state [29], and p53 mutations that impair its oligomerization have been associated with the Li-Fraumeni syndrome [30, 31]. Because HERC2 interacts with p53 and modulates its transcriptional activity by regulating its oligomerization [32] and *Herc2*^{+/⁵³⁰} mice have less p53 activity (Figure 5), we would expect *Herc2*^{+/⁵³⁰} mice to show an increased susceptibility to developing spontaneous tumors. However, we have not observed a greater number of tumors in *Herc2*⁵³⁰ mice (data not shown). In agreement with these data, an increased susceptibility to develop spontaneous tumors in individuals from the Amish community with the HERC2^{P594L} punctual mutation [4,5] and lower p53 activity (Figure 6) has not been reported. The hypothesis that loss of transcription in p53 is the driving force selected during tumorigenesis needs to be reevaluated, as it is far from straightforward. For example, mice expressing p53 mutants transcriptionally defective for growth arrest, senescence and apoptosis, are not prone to cancer [39,40].

Moreover, cells from mice deficient for the three p53 target genes, *p21*, *Puma* and *Noxa*, are deficient in their ability to undergo p53-mediated cell-cycle arrest, apoptosis, and senescence, although the animals remain tumor-free [41].

Our study identifies a new function for the HERC2 ubiquitin ligase as a regulator of motor coordination through regulation of Purkinje cells homeostasis. HERC2 protein is expressed in Purkinje cells (Figure 9). The decrease of its protein levels correlates with the loss of Purkinje cells in the vermis and hemispheres of the cerebellum that would explain the motor incoordination detected in *Herc2*^{+/⁵³⁰} mice with rotarod experiments (Figures 7 and 8). The Purkinje cell loss is bilateral and symmetrical as in other mutations characterized by the Purkinje cells loss [42], demonstrating the specificity of the degenerative process. This loss is not homogeneously distributed; thus, the loss of Purkinje cells appears as discrete gaps in the continuous staining of the molecular layer of the vermis, while at the hemispheres, the loss reaches a great extension (Figure 8). Despite their homogenous shapes and common morphological features, these results suggest some difference between Purkinje cells and is in agreement with previous observations indicating that these neurons do not constitute a biochemically homogenous population [42,43]. Pathological signs, such as varicose enlargements resembling axonal torpedoes and widespread accumulations of dense cytoplasmic material, were observed in Purkinje cells of *Herc2*^{+/⁵³⁰} mice. Proliferation of Golgi epithelial cells is also indicative of Purkinje cell degeneration. Electron microscopy analysis of *Herc2*^{+/⁵³⁰} cerebella showed Purkinje cells containing numerous degenerating signs in autophagosomes, lysosomes and Golgi cisterns (Figure 10 and 11, and data not shown). These results resemble those obtained from a different mutant mouse called *tambaleante* [44,45]. In these animals, a progressive and specific loss of Purkinje cell was observed with a very similar pattern of neurodegenerative signs. Interestingly, the Purkinje cell degeneration in *tambaleante* mutant mice is a consequence of a missense mutation in HERC1 [44], the structural homolog of HERC2. In this regard, it seems that the functional alteration of one of them it is not compensated by the other. In agreement with this independent role of HERC1 and HERC2, the essential role of HERC1 for normal development and for neurotransmission at the mouse neuromuscular junction [46] was not observed in *Herc2*^{+/⁵³⁰} mice (Figure 7). Thus, both ubiquitin ligases seem to have a crucial and independent role in Purkinje cell physiology. This functional similarity of HERC1 and HERC2 was unexpected, because despite their structural homology, endogenous proteins do not interact between them, do not have common known interactors, have different subcellular locations and were involved in different pathways of cell signaling [11, 12, 32]. However,

an interaction between the first 1,000 amino acid residues of HERC2 and HERC1 has recently been detected using mass spectrometry analysis [47], suggesting a possible interaction in some unknown circumstances.

A functional role of cerebellar p53 protein in adult walking synchronization has been reported [48]. Because HERC2 positively regulates p53 activity [32] and *Herc2*^{+/⁵³⁰} mice had less HERC2 activity, it was plausible that the impaired motor synchronization in *Herc2*^{+/⁵³⁰} mice was caused by a decrease in p53 activity. For this reason, we analyzed motor coordination in p53 knockout mice. We did not observe significant differences with rotarod experiments in these animals (Figure 7). Our results are in agreement with other studies where no differences in motor synchronization were detected by Tomasevic *et al.* [49] in p53 knockout mice. These authors described a role for p53 in the recovery of neuromotor function after a traumatic brain injury but not before the injury [49]. Thus, the motor coordination regulated by HERC2 seems to be independent of p53 activity.

Pioneering studies associated mutations at the mouse *Herc2* locus induced by ethylnitrosourea or ionizing radiation with a runty, jerky, sterile phenotype (*rjs*), also known as the juvenile development and fertility phenotype (*jfd2*), characterized by reduced size, jerky gait, fertility problems, including spermatocyte and oocyte abnormalities, defective maternal behaviour, and reduced lifespan with juvenile lethality [50-52]. More recently, a mutation in the *HERC2* gene has been linked to the neurodevelopmental delay and dysfunction seen in Angelman syndrome and autism-spectrum disorders among the Amish community [4, 5]. Now, our study demonstrates an important role of HERC2 in the regulation of motor coordination through Purkinje cells homeostasis that would explain some features observed in *rjs/jfd2* mice and individuals with the *HERC2*^{P594L} mutation. It is important to note that, different to the above studies, the impaired motor synchronization is observed in mice with only a mutated allele of *Herc2* (*Herc2*^{+/⁵³⁰} mice), indicating the relevance of HERC2 activity in motor function coordination.

Studies of spontaneous mouse mutants have implicated autophagy in the death of Purkinje neurons. *Lurcher* mice with mutations in the delta2 glutamate receptor, *pcd* mice with loss of *nnal* expression or *tambaleante* mice with mutation in the HERC1 protein show an increase of autophagy associated with Purkinje cell death [44, 53-55]. While conditional inactivation of autophagy genes such as *Atg5* or *Atg7* from Purkinje cells in mice yields Purkinje cell degeneration and death [56, 57]. This dual role of the autophagy in Purkinje cells degeneration seems to indicate that these neurons are very sensitive to the dysregulation of autophagy. Although more studies will be necessary to establish the role precise of HERC2 in autophagy, our results are in agreement with these previous observations in other mouse models, and

reveal a dysregulation of autophagy in *Herc2*^{+/⁵³⁰} Purkinje cells. A recent study also suggests the involvement of HERC2 in Parkinson's disease [58], it would be interesting to analyze in future studies the HERC2 role in the midbrain dopaminergic neurons of *Herc2*^{+/⁵³⁰} mice.

In summary, the generation of a mutant mouse of *Herc2* led us to identify the HERC2 ubiquitin ligase as essential for embryonic development and an important regulator of motor coordination. These results may also explain some features observed among the Old Order Amish with a homozygous missense mutation in *HERC2*. Future studies will be necessary to identify additional partners involved in HERC2 physiology and its role in human diseases.

MATERIALS AND METHODS

Animals

The ES cell line AR0530 from The Sanger Institute containing a gene trap β -galactosidase/neomycin (β -geo-Neo) cassette that has integrated between exons 2 and 3 in the *Herc2* gene was used. We choose this ES cell line to study *Herc2* gene expression by β -galactosidase activity and to avoid the variability of the already existing *Herc2* mutations (deletions, point mutations, DNA rearrangements) [50]. ES cells were injected into 4.5 day C57BL/6J blastocysts, which were then implanted into pseudopregnant females. The resulting 90-95% coat color chimeras were crossed with C57BL/6 mice to generate the heterozygous animals *Herc2*/*Herc2*⁵³⁰ (*Herc2*^{+/⁵³⁰}). *p53* knockout mice B6.129S2-*Trp53*^{tm1Tyj}/J from Jackson laboratories [37] were kindly provided by Dr. J. Martin-Caballero. All animal experiments were performed in accordance with guidelines approved by the Ethical Committee for Animal Experimentation of the University of Barcelona.

Genotyping

Tail DNA or embryo samples were purified using the NucleoSpin Tissue kit (MACHEREY-NAGEL) according to the manufacturer's protocol. PCR amplification was performed using the primers: 530KO1 5'GGCTGCCAGTCTCGCCTTG3' and 530KO04 5'CTGTCACCTCTCCGGGAGAAC3' for the amplification of the *Herc2* wild-type allele; Gal7 5'TTTCCATATGGGGATTGGTG3' and Gal8 5'TGTCTGTTGTGCCAGTCAT3' for the *Herc2* 530 allele; and p53036 5'ACAGCGTGGTGGTACCT3' and p53037 5'TATACTCAGAGCCGGCCT p53038 5'CTATCAAGGCATAGCGTTGG for the genotype of p53. The PCR settings were 94°C for 3 minutes, 94°C for 1 minute, annealing at 60°C for 1 minute and elongation at

72°C for 1 minute, for 35 cycles.

RT-PCR

To assess trap expression, total RNA was isolated from mice tissues or cells using TRIreagent (Bioline). Two µg of total RNA was reverse-transcribed using the cDNA Reverse Transcription kit (Applied Biosystems) and random primers. To assess the trap insertion, PCR was carried out with primers: 530KO02 5' CAGGTCTGACCACCCGGAGG3'; 530KO09 5' GGGAGTTCTCGATTTTGTGC3'; and β-geo40/60 5' AGGGTTTTCCAGTCACGAC3'. The PCR settings were 94°C for 3 minutes, 94°C for 1 minute, annealing at 55°C for 30 seconds and elongation at 72°C for 45 seconds, for 30 cycles. Additionally, cDNA was sequenced using BigDye 3.1 on an ABI 3130XL genetic analyzer (Applied Biosystems). To analyze the expression of *p21*, RT quantitative PCR was carried out using the ABI Prism 7900 HT fast-real Time PCR system and commercially available Taqman assays (Applied Biosystems): *CDKN1A* (mouse p21: Mm04205640_g1; human p21: Hs00355783_m1); *GAPDH* (mouse GAPDH: Mm99999915_g1; human GAPDH: Hs99999905_m1); and *18S* (Hs99999901_s1). The PCR data were captured and analyzed using the Sequence Detector software (SDS version 2.3, Applied Biosystems).

Histology and immunohistochemistry

X-gal staining of β-galactosidase activity. Mice were anesthetized and perfused via the left ventricle with 2% paraformaldehyde in a phosphate buffer (0.12 M). All tissues were dissected and fixed in the same solution for 3 hours at 4°C, and later were cryopreserved by immersion in 30% sucrose for 48 h at 4°C. Whole tissues were then embedded into an 8% gelatin and 15% sucrose solution, frozen in liquid nitrogen and stored at -80°C. Before staining for β-galactosidase activity, the tissues were sliced (7-10 µm), prepared on polylysinated slides, and permeabilized with PBS-0.3% Triton. After washing in PBS, the slices were incubated in staining solution (2 mM *X-gal*, 4 mM K₄Fe(CN)₆, 4 mM K₃Fe(CN)₆, 2 mM MgCl₂ in PBS) overnight while shaking in the dark at 4°C. After washing in PBS, the slices were stained with neutral red and mounted for microscopic observation.

The protocol to study the cerebellar Purkinje cells was reported previously [46]. Briefly, two and nine month old mice were deeply anaesthetised with pentobarbital (80 mg/kg i.p.), and perfused transcardially with 4% paraformaldehyde in 0.12 M phosphate buffer (PB, pH 7.2). After dissection, the brains were post-fixed overnight in the same fixative and transferred to 30% sucrose in PB until they sank. Sagittal and coronal sections of the cerebellum (40 µm thick) were cut on a

freezing microtome, and collected in PBS. The sections were incubated overnight with a polyclonal anti-calbindin D-28k antibody (1:10,000). After washing, the sections were incubated for one hour in a biotinylated secondary antibody (1:500) followed by incubation for one hour in the ABC elite kit (1:400). A mixture of 0.3% DAB-0.6% nickel sulfate-0.1% hydrogen peroxide in PBS was used to reveal the immunoreaction. For double labeling analyses the sections were incubated overnight with the following primary antibodies mixtures: polyclonal anti-HERC2 (1:400)/monoclonal anti-calbindin D-28k (1:1000), and polyclonal anti-HERC2 (1:400)/monoclonal anti-p62 (1:100). After washing, the sections were incubated for one hour in a mixture of Alexa Fluor® 488 donkey-anti-rabbit (1:500) and Alexa Fluor® 594 donkey-anti-mouse (1:500). Images were acquired in a Zeiss Axio-Imager M1 microscope. Laser confocal analyses were made on an Olympus FluoView 1000 upright microscope.

Electron microscopy

Two and nine month old mice were deeply anaesthetized with pentobarbital (80 mg/kg i.p.), and perfused transcardially with a mixture of 1% paraformaldehyde and 1% glutaraldehyde in 0.12 M phosphate buffer (PB, pH 7.2). Thereafter, the brains were dissected out and immersed overnight in the same fixative. Sagittal slices of the cerebella were cut and immersed in 2% OsO₄ in PB, stained in a block with ethanolic 0.5% uranyl acetate, dehydrated with an increased gradient of ethanol, and embedded in Durcupan (Fluka®). Semithin and ultrathin sections were obtained on a Leica EM UC7 ultramicrotome. Semithin sections were stained with 1% toluidine blue. Ultrathin sections were collected in copper grids (150 and 300 mesh) and observed without counterstaining in a Zeiss Libra EM at 80 kV (CITIUS).

Behavioural tests

Anxiety

To evaluate mice anxiety, two different protocols were used [59]. Tail suspension: mice were suspended above the floor by fixing the end of the tail to wire netting and immobility was scored by manual observation during a 5 min test session. Time outside the dark box: mice were placed in a rectangular arena (55x40x40 cm³) with a dark box with a door. The time inside/outside the box was scored by manual observation during a 5 min test session.

Learning and memory

Object recognition memory

Mice were tested as described previously [60]. Briefly, mice were placed in a rectangular arena (55x40x40 cm³) and two identical objects were placed in the arena during the training phase. Subsequently, the animal's memory of one of the original objects was assessed by comparing the amount of time spent exploring the novel object as compared with that spent exploring the familiar one. The relative exploration of the novel object was expressed as a discrimination index $[DI = 5(t_{\text{novel}} - t_{\text{familiar}}) / (t_{\text{novel}} + t_{\text{familiar}})]$.

Step-through passive avoidance test

The test was performed as described previously [60]. Briefly, in the habituation phase, the mice were handled and allowed to move freely for 1 min in a chamber (47x18x26 cm³, manufactured by Ugo Basile). In the training phase, the mice were confined to the light compartment and then 30 s later, the door separating the dark-light compartments was opened. Once mice entered the dark compartment, the door closed automatically and the mice received an electrical stimulation (0.5 mA, 5 s) delivered through the metal floor. In the retention tests, the latency to enter into a dark compartment (escape latency) is a measure of information learning or memory retention. To compare the results obtained in different experiments, the fold change in escape latency with respect to the latency obtained in the training session is calculated.

Motor function

Motor activity in the open field

To evaluate locomotor and exploratory activity, mice were placed for 5 minutes in an open field (38x21x15 cm) (Cybertec S.A.). This apparatus consisted of a walled platform containing infrared emitters and sensors (IR) coupled to an altimeter, and the movement sensor was connected to a computer that recorded the number of times the mouse interrupted the IR beams/min.

Fore limb grip strength

To evaluate fore limb strength, mice were held above a horizontal wire and lowered to allow the fore limbs to grip the wire. The ability of the mice to remain attached by the fore limbs was scored during 10 s.

Rotarod

To habituate mice to the rotarod (Ugo Basile Biological Research Apparatus), the animals were placed on the roller at a speed of 20 rpm until they could remain on it for one minute without falling off. To assay motor

coordination, animals were then tested at a rotational speed of 20 rpm, accelerating to 60 rpm in increments of 5 rpm, and quantifying the number of falls at each increase in speed.

Electrophysiological analysis of the medial gastrocnemius (MG) muscle in mice

Compound muscular action potentials (CMAPs) were recorded in anesthetized mice (tribromethanol 2 %, 0.15 ml/10 g body weight, i.p.) as described previously [46,61]. Briefly, the recording needle electrode was placed into the medial part of the MG muscle and the reference electrode was situated at the base of the fifth phalanx. A ground electrode was placed at the base of the tail. Stimulating needle electrodes were placed at the sciatic notch and the head of the fibula. Stimulation protocols of supramaximal current pulses (0.05 ms duration, 5-10 mA amplitude) were applied as a short train of 100 Hz pulses generated by an isolated pulse stimulator (Pulse Train Stimulator Cibertec cs-20). The outputs recorded were differentially amplified (P511 AC Amplifier Astro-Med, INC), digitally acquired at 10,000 samples/s (CED 1401 Plus; Cambridge Electronic Designed, Cambridge, UK) and stored on a computer for later analysis. The analysis consisted of measuring the amplitude from the positive to the negative peak of the CMAPs recorded during a train of stimuli, normalizing the amplitude to the first response.

Cell culture and transfection

Human fibroblasts and ethical statements were previously described [5]. U2OS cells were obtained from ATCC. Cells were cultured at 37°C in Dulbecco's modified Eagle's medium (DMEM) supplemented with 10% fetal bovine serum, 100 units/ml penicillin, 100 µg/ml streptomycin and 2 mM glutamine. Transfection of cells with siRNAs (Non Targeting, NT: UAGCGACUAAACACAUCAA; HERC2, H2: GACUGUAGCCAGAUUGAAA) purchased from GenePharma was carried out using calcium phosphate. Transfected cells were analyzed 72 hours post-transfection. MG132 (Z-Leu-Leu-Leu-al) (Sigma-Aldrich) was added to the cells for 6 hours to a final concentration of 10 µM.

Antibodies used

The following antibodies were used: anti-HERC2 monoclonal (BD Biosciences); anti-HERC2 polyclonal [32]; anti-p21 (C-19); anti-p62 (SQSTM1 (D-3): sc-28359); anti-β-actin (Santa Cruz Biotechnology, Inc.); anti-calbindin D-28k polyclonal (Cb-38a, Swant); anti-calbindin D-28k monoclonal (Cb-955, Sigma); anti-p53

Ab-5 (DO-7) (Neo Markers); anti-USP33 (Proteintech); anti-Ran [62]; anti α -tubulin (Ab-1, Calbiochem); Alexa Fluor® 488 donkey-anti-rabbit (A21207), and Alexa Fluor® 594 donkey-anti-mouse (A21203) (Invitrogen); horseradish peroxidase-conjugated secondary antibodies (Invitrogen); biotin-conjugated secondary antibodies (Vector); and the Avidine-Streptavidine Elite Kit (Vector).

Lysate and immunoblot

Mice were euthanized by cervical dislocation. The organs were collected and frozen in liquid nitrogen and stored at -80°C until analysis. Tissues, human fibroblasts or U2OS cells were prepared in lysis buffer (consisting of 50 mM TrisHCl, pH 7.5, 150 mM NaCl, 0.5% NP40, 50 mM β -glycerophosphate, 50 mM NaF, 1 mM sodium vanadate, 1 mM phenyl-methylsulfonyl fluoride, 5 $\mu\text{g}/\text{mL}$ leupeptin, 5 $\mu\text{g}/\text{mL}$ aprotinin, 1 $\mu\text{g}/\text{mL}$ pepstatin-A and benzamidin 100 $\mu\text{g}/\text{mL}$) and the tissues were homogenized in a motor-driven Polytron PT3000. The lysates were incubated on ice for 20 minutes and centrifuged at 13,000 g for 10 minutes at 4°C . Total protein levels were measured by BCA (Pierce). Equal amounts of supernatant proteins were analyzed using the Tris-acetate PAGE system [63]. Band intensities were analyzed using a gel documentation system (LAS-3000, Fujifilm). Proteins levels were normalized and expressed as a percentage of controls.

Statistical analysis

The results are expressed as mean \pm SEM. The data were analyzed by one-way analysis of variance (ANOVA) or Student's *t*-test. For comparison of significance, Tukey's test was used as a post hoc test according to the statistical program GraphPad Prism. Differences were considered significant at *p* values of less than 0.05: **p* < 0.05, ***p* < 0.01, and ****p* < 0.001.

ACKNOWLEDGMENTS

We would like to thank The Sanger Institute for the ES cell line AR0530, J. Martin-Caballero for *p53*^{-/-} mice, and A. Gimeno, E. Adanero, A. Angelo, E. Castaño and B. Torrejon for technical assistance. We also acknowledge S. Sánchez-Tena for valuable discussion throughout this study, and G. Alvarez de Toledo for the facilities to use the FluoView 1000 laser confocal scanning microscope. RR held a Juan de la Cierva contract JCI-2011-08888 from the MINECO and VPPI-US from the University of Sevilla. TS and LP were supported by fellowships from the CAPES Foundation (Ministry of Education from Brazil) and from CNPq-Programa Ciências sem Fronteiras (Ministry of Science, Technology and Innovation Education of Brazil), respectively. This article is based upon work from COST

Action (PROTEOSTASIS BM1307), supported by COST (European Cooperation in Science and Technology).

CONFLICTS OF INTEREST

All authors have not conflicts of interest to disclose.

GRANT SUPPORT

This work was supported by grants from Spanish Ministerio de Ciencia e Innovación [BFU2011-22498 to J.L.R. and BFU2014-56313P to F.V.] and Brazilian Scientific Program “Ciências sem Fronteiras” from the Ministry of Science, Technology and Innovation Education of Brazil [313600/2013-9 to J.L.R. and 400422/2013-1 to J.R.O.].

Editorial note

This paper has been accepted based in part on peer-review conducted by another journal and the authors' response and revisions as well as expedited peer-review in Oncotarget.

REFERENCES

1. Williams CA, Beudet AL, Clayton-Smith J, Knoll JH, Kyllerman M, Laan LA, Magenis RE, Moncla A, Schinzel AA, Summers JA, Wagstaff J. Angelman syndrome 2005: updated consensus for diagnostic criteria. *Am J Med Genet A*. 2006; 140: 413-418.
2. Mabb AM, Judson MC, Zylka MJ, Philpot BD. Angelman syndrome: insights into genomic imprinting and neurodevelopmental phenotypes. *Trends Neurosci*. 2011; 34: 293-303.
3. Williams CA, Driscoll DJ, Dagi AI. Clinical and genetic aspects of Angelman syndrome. *Genet Med*. 2010; 12: 385-395.
4. Puffenberger EG, Jinks RN, Wang H, Xin B, Fiorentini C, Sherman EA, Degrazio D, Shaw C, Sougnez C, Cibulskis K, Gabriel S, Kelley RI, Morton DH, et al. A homozygous missense mutation in HERC2 associated with global developmental delay and autism spectrum disorder. *Hum Mutat*. 2012; 33: 1639-1646.
5. Harlalka G V, Baple EL, Cross H, Kuhnle S, Cubillos-Rojas M, Matentzoglou K, Patton MA, Wagner K, Coblentz R, Ford DL, Mackay DJ, Chioza BA, Scheffner M, et al. Mutation of HERC2 causes developmental delay with Angelman-like features. *J Med Genet*. 2013; 50: 65-73.
6. Cassidy SB, Schwartz S, Miller JL, Driscoll DJ. Prader-Willi syndrome. *Genet Med*. 2012; 14: 10-26.
7. Kuhnle S, Kogel U, Glockzin S, Marquardt A, Ciechanover A, Matentzoglou K, Scheffner M. Physical and functional interaction of the HECT ubiquitin-protein ligases E6AP and

- HERC2. *J Biol Chem.* 2011; 286: 19410-19416.
8. Pośpiech E, Draus-Barini J, Kupiec T, Wojas-Pelc A, Branicki W. Gene-gene interactions contribute to eye colour variation in humans. *J Hum Genet.* 2011; 56: 447-455.
 9. Mengel-From J, Børsting C, Sanchez JJ, Eiberg H, Morling N. Human eye colour and HERC2, OCA2 and MATP. *Forensic Sci Int Genet.* 2010; 4: 323-328.
 10. White D, Rabago-Smith M. Genotype-phenotype associations and human eye color. *J Hum Genet.* 2011; 56: 5-7.
 11. Garcia-Gonzalo FR, Rosa JL. The HERC proteins: functional and evolutionary insights. *Cell Mol Life Sci.* 2005; 62: 1826-38.
 12. Hadjebi O, Casas-Terradellas E, Garcia-Gonzalo FR, Rosa JL. The RCC1 superfamily: From genes, to function, to disease. *Biochimica et Biophysica Acta.* 2008; 1783: 1467-1479.
 13. Dastur A, Beaudenon S, Kelley M, Krug RM, Huibregtse JM. Herc5, an interferon-induced HECT E3 enzyme, is required for conjugation of ISG15 in human cells. *J Biol Chem.* 2006; 281: 4334-4338.
 14. Kroismayr R, Baranyi U, Stehlik C, Dorfleutner A, Binder BR, Lipp J. HERC5, a HECT E3 ubiquitin ligase tightly regulated in LPS activated endothelial cells. *J Cell Sci.* 2004; 117: 4749-4756.
 15. Hochrainer K, Kroismayr R, Baranyi U, Binder BR, Lipp J. Highly homologous HERC proteins localize to endosomes and exhibit specific interactions with hPLIC and Nm23B. *Cell Mol Life Sci.* 2008; 65: 2105-2117.
 16. Diouf B, Cheng Q, Krynetskaia NF, Yang W, Cheok M, Pei D, Fan Y, Cheng C, Krynetskiy EY, Geng H, Chen S, Thierfelder WE, Mullighan CG, et al. Somatic deletions of genes regulating MSH2 protein stability cause DNA mismatch repair deficiency and drug resistance in human leukemia cells. *Nat Med.* 2011; 17: 1298-1303.
 17. Bekker-Jensen S, Rendtlew Danielsen J, Fugger K, Gromova I, Nerstedt A, Lukas C, Bartek J, Lukas J, Mailand N. HERC2 coordinates ubiquitin-dependent assembly of DNA repair factors on damaged chromosomes. *Nat Cell Biol.* 2010; 12: 12-80.
 18. Yoo NJ, Park SW, Lee SH. Frameshift mutations of ubiquitination-related genes HERC2, HERC3, TRIP12, UBE2Q1 and UBE4B in gastric and colorectal carcinomas with microsatellite instability. *Pathology.* 2011; 43: 753-755.
 19. Zhou H, Shi R, Wei M, Zheng W-L, Zhou JY, Ma WL. The expression and clinical significance of HERC4 in breast cancer. *Cancer Cell Int.* 2013; 13: 113.
 20. Sánchez-Tena S, Cubillos-Rojas M, Schneider T, Rosa JL. Functional and pathological relevance of HERC family proteins: a decade later. *Cell Mol Life Sci.* 2016; 73: 1955-1968.
 21. Kang T-H, Lindsey-Boltz L a, Reardon JT, Sancar A. Circadian control of XPA and excision repair of cisplatin-DNA damage by cryptochrome and HERC2 ubiquitin ligase. *Proc Natl Acad Sci U S A.* 2010; 107: 4890-4895.
 22. Wu W, Sato K, Koike A, Nishikawa H, Koizumi H, Venkitaraman AR, Ohta T. HERC2 is an E3 ligase that targets BRCA1 for degradation. *Cancer Res.* 2010; 70: 6384-6392.
 23. Oestergaard VH, Pentzold C, Pedersen RT, Iosif S, Alpi A, Bekker-Jensen S, Mailand N, Lisby M. RNF8 and RNF168 but not HERC2 are required for DNA damage-induced ubiquitylation in chicken DT40 cells. *DNA Repair (Amst).* 2012; 11: 892-905.
 24. Al-Hakim AK, Bashkurov M, Gingras AC, Durocher D, Pelletier L. Interaction Proteomics Identify NEURL4 and the HECT E3 Ligase HERC2 as Novel Modulators of Centrosome Architecture. *Mol Cell Proteomics.* 2012; 11: M111.014233.
 25. Chan NC, Den Besten W, Sweredoski MJ, Hess S, Deshaies RJ, Chan DC. Degradation of the deubiquitinating enzyme USP33 is mediated by p97 and the ubiquitin ligase HERC2. *J Biol Chem.* 2014; 289: 19789-19798.
 26. Moroishi T, Yamauchi T, Nishiyama M, Nakayama KI. HERC2 targets the iron regulator FBXL5 for degradation and modulates iron metabolism. *J Biol Chem.* 2014; 289: 16430-16441.
 27. Brady CA, Attardi LD. P53 at a Glance. *J Cell Sci.* 2010; 123: 2527-2532.
 28. Kruse JP, Gu W. Modes of p53 Regulation. *Cell.* 2009; 137: 609-622.
 29. Itahana Y, Ke H, Zhang Y. p53 Oligomerization is essential for its C-terminal lysine acetylation. *J Biol Chem.* 2009; 284: 5158-5164.
 30. Davison TS, Yin P, Nie E, Kay C, Arrowsmith CH. Characterization of the oligomerization defects of two p53 mutants found in families with Li-Fraumeni and Li-Fraumeni-like syndrome. *Oncogene.* 1998; 17: 651-656.
 31. Lomax ME, Barnes DM, Hupp TR, Picksley SM, Camplejohn RS. Characterization of p53 oligomerization domain mutations isolated from Li-Fraumeni and Li-Fraumeni like family members. *Oncogene.* 1998; 17: 643-649.
 32. Cubillos-Rojas M, Amair-Pinedo F, Peiró-Jordán R, Bartrons R, Ventura F, Rosa JL. The E3 ubiquitin protein ligase HERC2 modulates the activity of tumor protein p53 by regulating its oligomerization. *J Biol Chem.* 2014; 289: 14782-14795.
 33. Jones SN, Roe AE, Donehower LA, Bradley A. Rescue of embryonic lethality in Mdm2-deficient mice by absence of p53. *Nature.* 1995; 378: 206-208.
 34. Parant J, Chavez-Reyes A, Little NA, Yan W, Reinke V, Jochemsen AG, Lozano G. Rescue of embryonic lethality in Mdm4-null mice by loss of Trp53 suggests a nonoverlapping pathway with MDM2 to regulate p53. *Nat Genet.* 2001; 29: 92-95.

35. Montes de Oca Luna R, Wagner DS, Lozano G. Rescue of early embryonic lethality in mdm2-deficient mice by deletion of p53. *Nature*. 1995; 378: 203-206.
36. Donehower LA, Harvey M, Slagle BL, McArthur MJ, Montgomery CA, Butel JS, Bradley A. Mice deficient for p53 are developmentally normal but susceptible to spontaneous tumours. *Nature*. 1992; 356: 215-221.
37. Jacks T, Remington L, Williams BO, Schmitt EM, Halachmi S, Bronson RT, Weinberg RA. Tumor spectrum analysis in p53-mutant mice. *Curr Biol*. 1994; 4: 1-7.
38. Donehower L a, Lozano G. 20 Years Studying P53 Functions in Genetically Engineered Mice. *Nat Rev Cancer*. 2009; 9: 831-41.
39. Li T, Kon N, Jiang L, Tan M, Ludwig T, Zhao Y, Baer R, Gu W. Tumor suppression in the absence of p53-mediated cell-cycle arrest, apoptosis, and senescence. *Cell*. 2012; 149: 1269-1283.
40. Brady CA, Jiang D, Mello SS, Johnson TM, Jarvis LA, Kozak MM, Broz DK, Basak S, Park EJ, McLaughlin ME, Karnezis AN, Attardi LD. Distinct p53 transcriptional programs dictate acute DNA-damage responses and tumor suppression. *Cell*. 2011; 145: 571-583.
41. Valente LJ, Gray DHD, Michalak EM, Pinon-Hofbauer J, Egle A, Scott CL, Janic A, Strasser A. p53 efficiently suppresses tumor development in the complete absence of its cell-cycle inhibitory and proapoptotic effectors p21, Puma, and Noxa. *Cell Rep*. 2013; 3: 1339-1345.
42. Dusart I, Guenet JL, Sotelo C. Purkinje cell death: differences between developmental cell death and neurodegenerative death in mutant mice. *Cerebellum*. 2006; 5: 163-173.
43. Hawkes R, colonnier M, Leclerc N. Monoclonal antibodies reveal sagittal banding in the rodent cerebellar cortex. *Brain Res*. 1985; 333: 359-365.
44. Mashimo T, Hadjebi O, Amair-Pinedo F, Tsurumi T, Langa F, Serikawa T, Sotelo C, Guenet JL, Rosa JL. Progressive Purkinje cell degeneration in tambaleante mutant mice is a consequence of a missense mutation in HERC1 E3 ubiquitin ligase. *PLoS Genet*. 2009; 5: e1000784.
45. Ruiz R, Pérez-Villegas EM, Bachiller S, Rosa JL, Armengol JA. HERC 1 Ubiquitin Ligase Mutation Affects Neocortical, CA3 Hippocampal and Spinal Cord Projection Neurons: An Ultrastructural Study. *Front Neuroanat*. 2016; 10: 42.
46. Bachiller S, Rybkina T, Porras-García E, Pérez-Villegas E, Tabares L, Armengol JA, Carrión AM, Ruiz R. The HERC1 E3 Ubiquitin Ligase is essential for normal development and for neurotransmission at the mouse neuromuscular junction. *Cell Mol Life Sci*. 2015; 72: 2961-2971.
47. Galligan JT, Martinez-Noël G, Arndt V, Hayes S, Chittenden TW, Harper JW, Howley PM. Proteomic analysis and identification of cellular interactors of the giant ubiquitin ligase HERC2. *J Proteome Res*. 2015; 14: 953-966.
48. Campana ALM, Rondi-Reig L, Tobin C, Lohof AM, Picquet F, Falempin M, Weitzman JB, Mariani J. p53 inactivation leads to impaired motor synchronization in mice. *Eur J Neurosci*. 2003; 17: 2135-2146.
49. Tomasevic G, Raghupathi R, Scherbel U, Wieloch T, McIntosh TK. Deletion of the p53 tumor suppressor gene improves neuromotor function but does not attenuate regional neuronal cell loss following experimental brain trauma in mice. *J Neurosci Res*. 2010; 88: 3414-3423.
50. Walkowicz M, Ji Y, Ren X, Horsthemke B, Russell LB, Johnson D, Rinchik EM, Nicholls RD, Stubbs L. Molecular characterization of radiation- and chemically induced mutations associated with neuromuscular tremors, runting, juvenile lethality, and sperm defects in jdf2 mice. *Mamm Genome*. 1999; 10: 870-878.
51. Ji Y, Walkowicz MJ, Buiting K, Johnson DK, Tarvin RE, Rinchik EM, Horsthemke B, Stubbs L, Nicholls RD. The ancestral gene for transcribed, low-copy repeats in the Prader-Willi/Angelman region encodes a large protein implicated in protein trafficking, which is deficient in mice with neuromuscular and spermiogenic abnormalities. *Hum Mol Genet*. 1999; 8: 533-542.
52. Lehman AL, Nakatsu Y, Ching A, Bronson RT, Oakey RJ, Keiper-Hrynko N, Finger JN, Durham-Pierre D, Horton DB, Newton JM, Lyon MF, Brilliant MH. A very large protein with diverse functional motifs is deficient in rjs (runty, jerky, sterile) mice. *Proc Natl Acad Sci U S A*. 1998; 95: 9436-9441.
53. Yue Z, Horton A, Bravin M, DeJager PL, Selimi F, Heintz N. A novel protein complex linking the $\delta 2$ glutamate receptor and autophagy: Implications for neurodegeneration in lurcher mice. *Neuron*. 2002; 35: 921-933.
54. Selimi F, Lohof AM, Heitz S, Lalouette A, Jarvis CI, Bailly Y, Mariani J. Lurcher GRID2-induced death and depolarization can be dissociated in cerebellar Purkinje cells. *Neuron*. 2003; 37: 813-819.
55. Chakrabarti L, Eng J, Ivanov N, Garden GA, La Spada AR. Autophagy activation and enhanced mitophagy characterize the Purkinje cells of pcd mice prior to neuronal death. *Mol Brain*. 2009; 2: 24.
56. Nishiyama J, Miura E, Mizushima N, Watanabe M, Yuzaki M. Aberrant membranes and double-membrane structures accumulate in the axons of Atg5-null Purkinje cells before neuronal death. *Autophagy*. 2007; 3: 591-596.
57. Komatsu M, Wang QJ, Holstein GR, Friedrich VL, Iwata J, Kominami E, Chait BT, Tanaka K, Yue Z. Essential role for autophagy protein Atg7 in the maintenance of axonal homeostasis and the prevention of axonal degeneration. *Proc Natl Acad Sci U S A*. 2007; 104: 14489-14494.
58. Imai Y, Kobayashi Y, Inoshita T, Meng H, Arano T, Uemura K, Asano T, Yoshimi K, Zhang CL, Matsumoto G, Ohtsuka T, Kageyama R, Kiyonari H, et al. The Parkinson's Disease-Associated Protein Kinase LRRK2 Modulates Notch Signaling through the Endosomal Pathway. *PLoS Genet*. 2015; 11:e1005503.

59. Romero-Granados R, Fontán-Lozano Á, Aguilar-Montilla FJ, Carrión ÁM. Postnatal proteasome inhibition induces neurodegeneration and cognitive deficiencies in adult mice: a new model of neurodevelopment syndrome. *PLoS One*. 2011; 6: e28927.
60. Suárez-Pereira I, Canals S, Carrión AM. Adult newborn neurons are involved in learning acquisition and long-term memory formation: the distinct demands on temporal neurogenesis of different cognitive tasks. *Hippocampus*. 2015; 25: 51-61.
61. Ruiz R, Tabares L. Neurotransmitter release in motor nerve terminals of a mouse model of mild spinal muscular atrophy. *J Anat*. 2014; 224: 74-84.
62. Rosa JL, Casaroli-Marano RP, Buckler AJ, Vilaro S, Barbacid M. p619, a giant protein related to the chromosome condensation regulator RCC1, stimulates guanine nucleotide exchange on ARF1 and Rab proteins. *EMBO J*. 1996; 15: 4262-4273.
63. Cubillos-Rojas M, Amair-Pinedo F, Tato I, Bartrons R, Ventura F, Rosa JL. Simultaneous electrophoretic analysis of proteins of very high and low molecular mass using Tris-acetate polyacrylamide gels. *Electrophoresis*. 2010; 31: 1318-1321.